Correlated signals of first-order phase transition in dark sector

Po-Yan Tseng (*NTHU*)
Danny Marfatia (*U. of Hawaii*)

References:
JHEP11(2021)068, arXiv:2107.00859, 2112.14588

2022 CAU Beyond the Standard Model Workshop Feb. 7-10, 2022

Introduction

- 125 GeV Higgs gives the mass to the SM particles through **spontaneous symmetry breaking**.

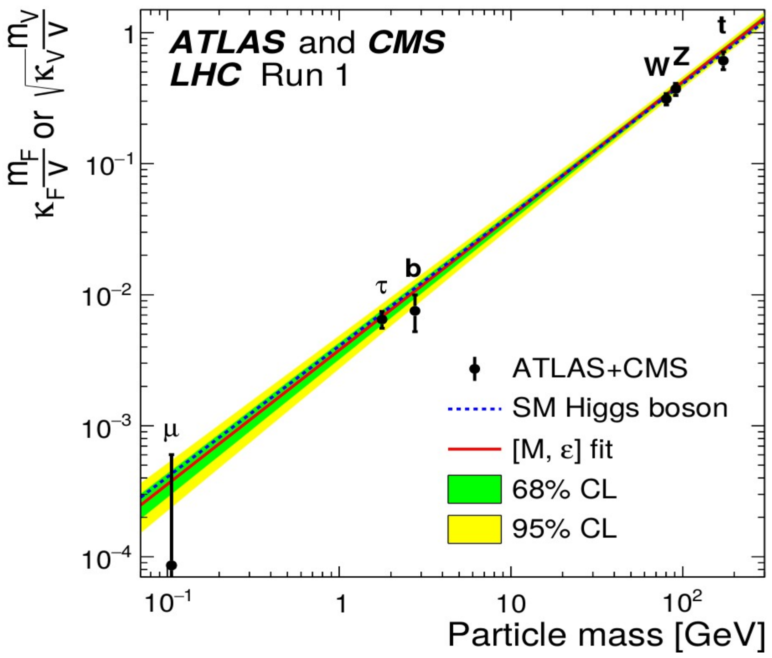

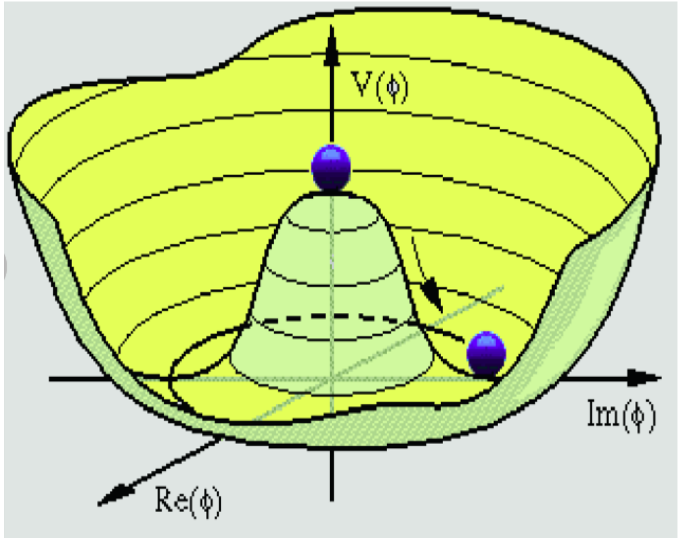

Dezso Horvath: Higgs and BSM studies at the LHC

Introduction

- Universe been through an **electroweak (QCD) phase transition** at T~100 GeV (100 MeV)

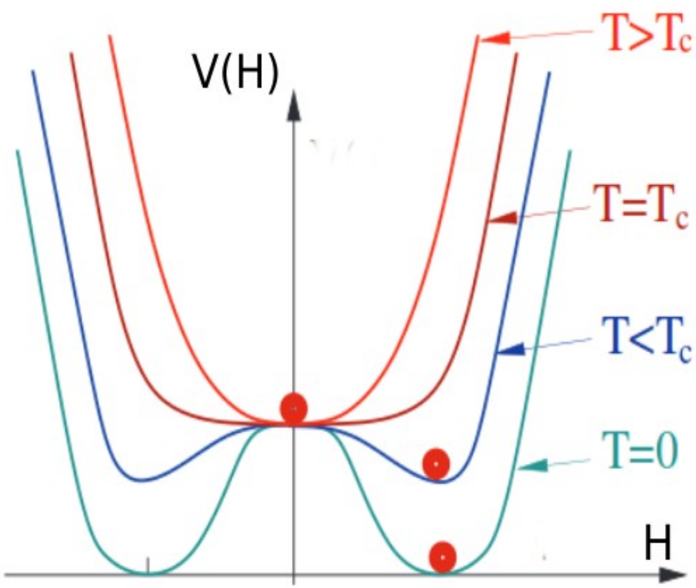

Cross over

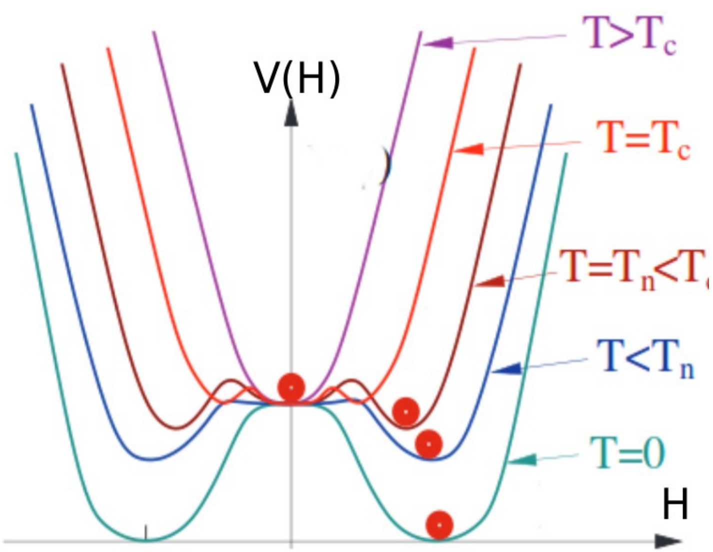

1st order

IN2P3

[PDF] Higgs potential and fundamental physics

Introduction

- Universe been through an **electroweak (QCD) phase transition** at T~100 GeV (100 MeV)

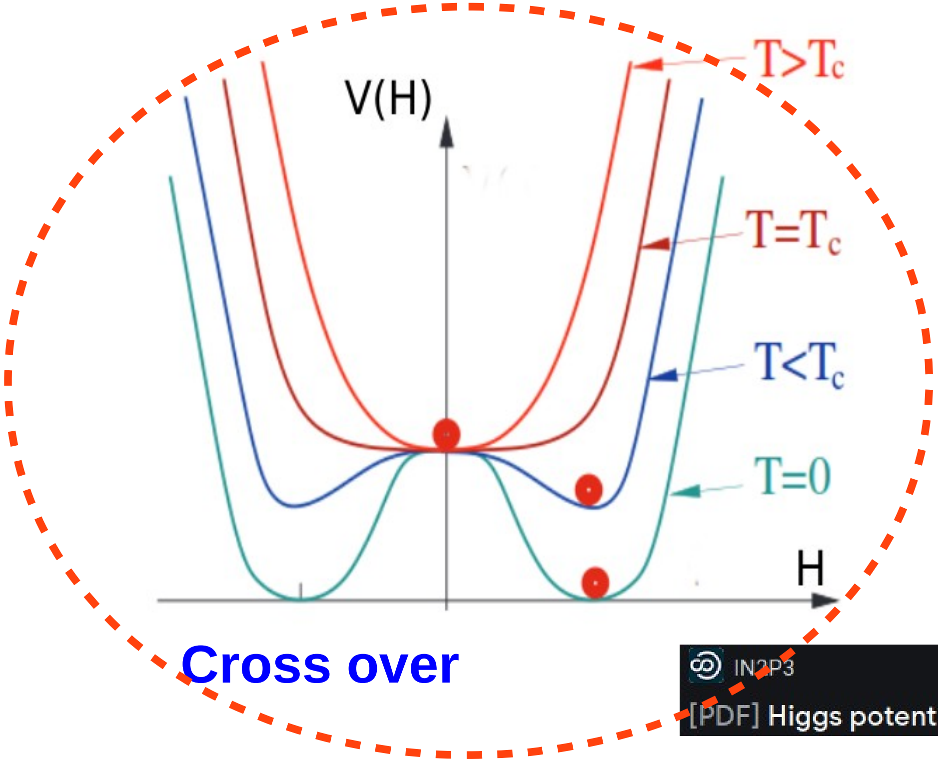

Cross over

IN2P3
[PDF] Higgs potential and fundamental physics

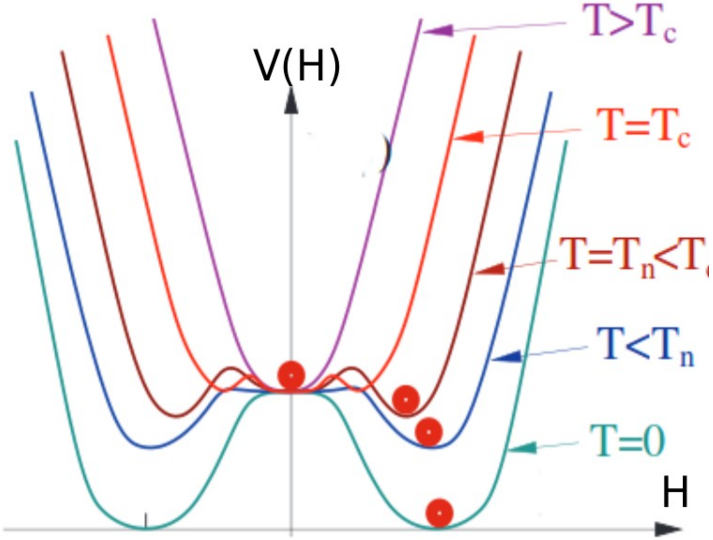

1st order

Introduction

- The origin of DM mass may come from the **spontaneous symmetry breaking** inducing by another scalar.

$$\mathcal{L} \supset \bar{\chi} i \partial\!\!\!/ \chi - g_\chi \phi \bar{\chi}\chi - V_{\rm eff}(\phi, T)$$

$$m_\chi \simeq g_\chi \langle \phi \rangle$$

- We consider **1st order phase transition (FOPT)**.

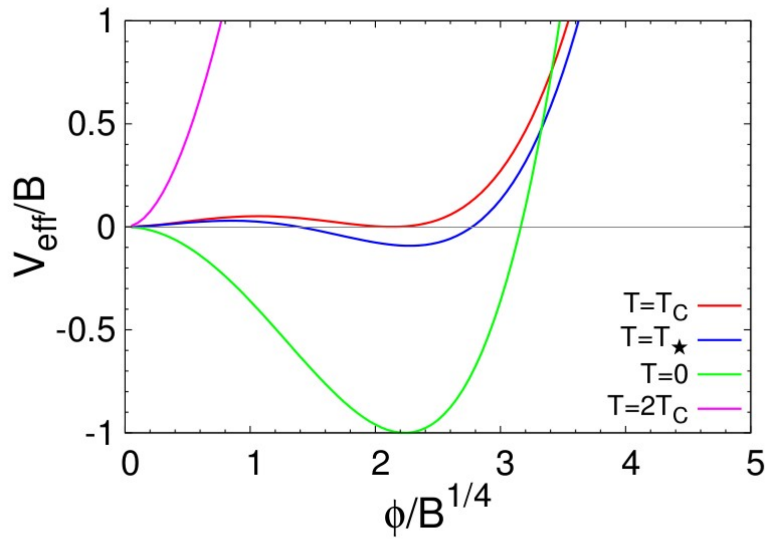

D.Marfatia, P.Y.Tseng

Introduction

- More rich phenomenologies, if we consider **1^{st} order phase transition (FOPT)**.

J.P.Hong, S.Jung, K.P.Xie: 2008.04430

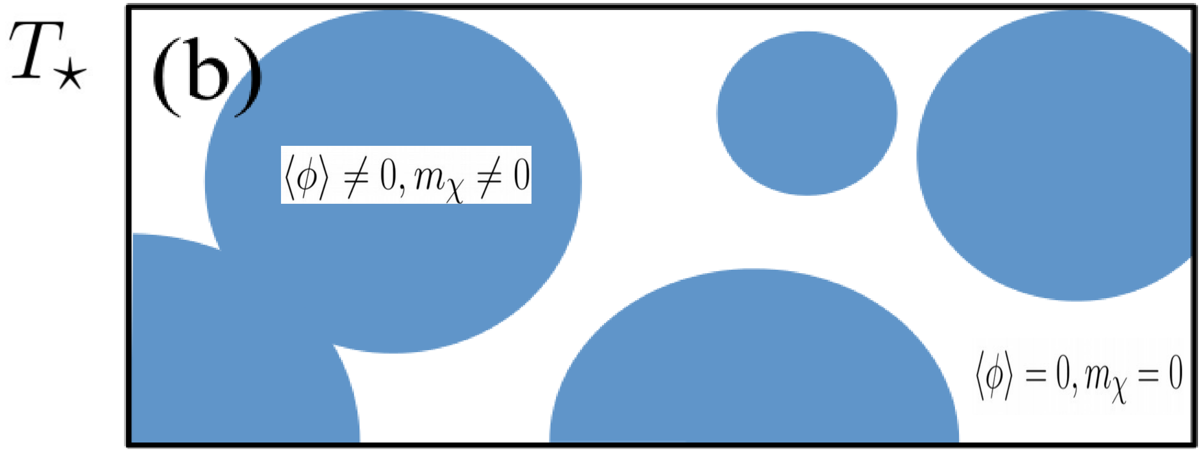

- DM particles **inside** the bubble becomes the DM relic density (bubble filtering DM: prof. C.S. Shin).

- DM particles **outside** the bubble could form macroscopic DM (Fermi Ball or primordial black hole)

Introduction

- More rich phenomenologies, if we consider **1st order phase transition (FOPT)**.

K.Kawana, K.P.Xie: 2106.00111

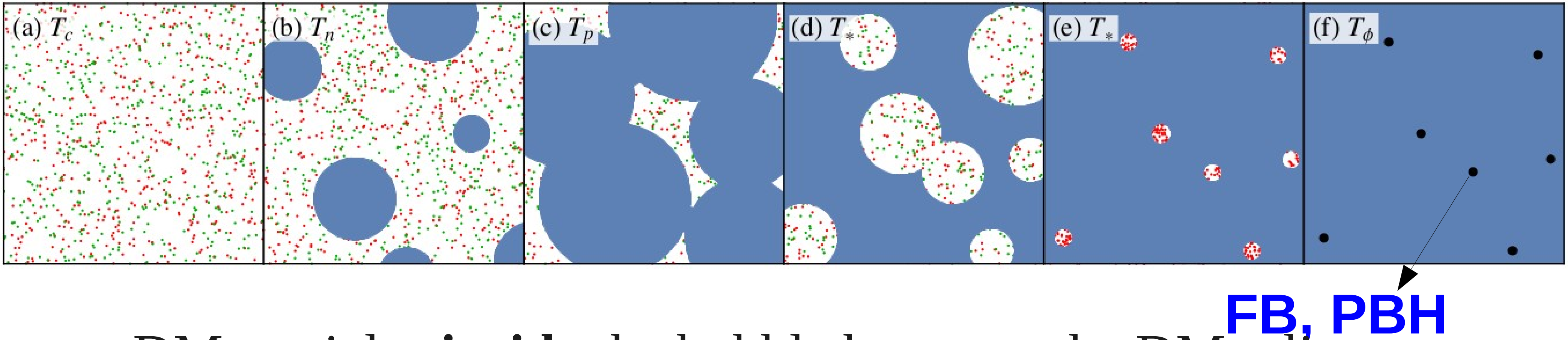

- DM particles **inside** the bubble becomes the DM relic density (bubble filtering DM: prof. C.S. Shin).

- DM particles **outside** the bubble could form macroscopic DM (Fermi Ball or primordial black hole)

Bubble filtering

- During FOPT, massless (massive) DM particles locate outside (inside) the bubble, and momentum conservation much be satisfied at the bubble wall.

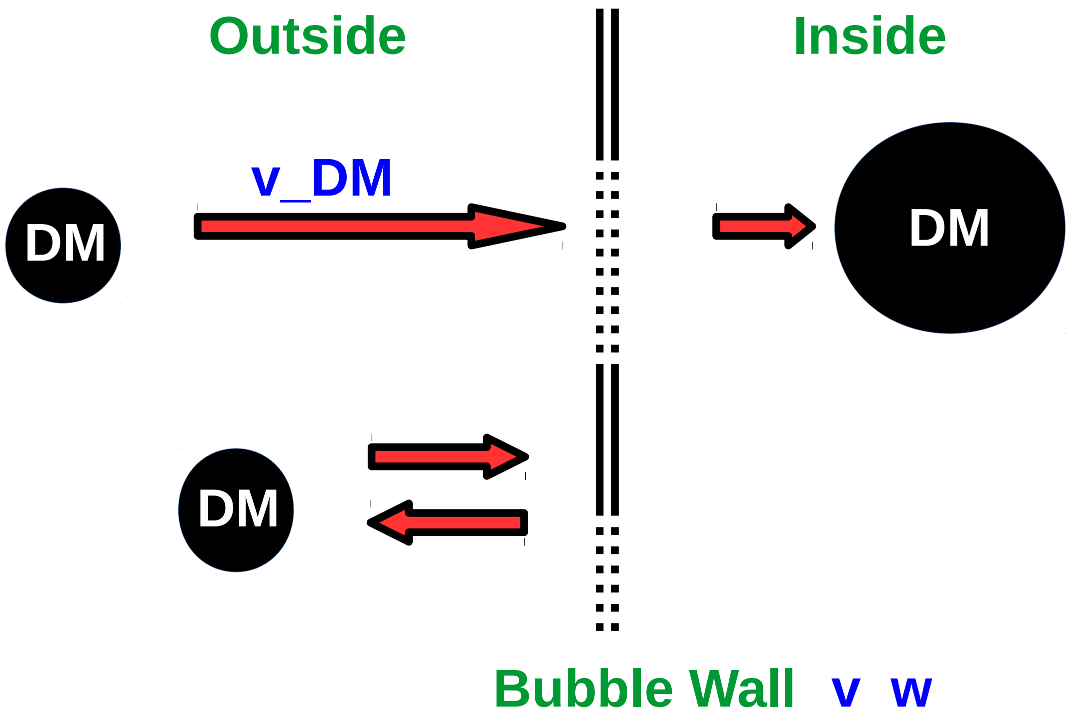

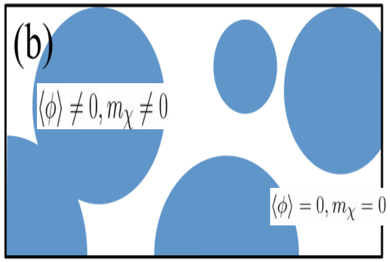

Bubble filtering

- Suppose DM particle mass is very heavy: $m_\chi \simeq g_\phi v_\phi \gg T_c$
- DM particles, remaining in **outside** the bubble (trapped in the *false vacuum*), will be aggregate by the expanding bubbles and form a macroscopic **Fermi-Ball(FB)**.
- For this to occur, there must be non-zero **asymmetry** $\eta_\chi \equiv (n_\chi - n_{\bar{\chi}})/s$ in the false vacuum so that the an excess remain after pair annihilation.
- The χ must carry a conserved global **U(1)_Q** charge so that **FB** attains stability

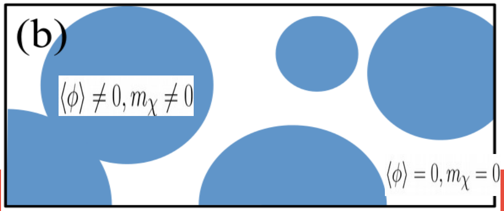

Number density of FB

- FBs start to form at $T_\star$ in the false vacuum, it shrinks and separates into smaller volumes.
- Critical volume $V_\star = 4\pi R_\star^3/3$, there is no other bubble forming inside during its shrinking $\Gamma(T_\star)V_\star\Delta t \sim 1$, corresponds to one FB.
- The number density of FB $n_{\rm FB}|_{T_\star}$ is determined by $n_{\rm FB}|_{T_\star} V_\star = F(t_\star)$:

$$n_{\rm FB}|_{T_\star} = \left(\frac{3}{4\pi}\right)^{1/4} \left(\frac{\Gamma(T_\star)}{v_w}\right)^{3/4} F(t_\star)$$

- The net Q-charge for a FB: $Q_{\rm FB} = \eta_\chi \left(\frac{s}{n_{\rm FB}}\right)_{T_\star}$

FB mass profile

- The mass and radius of FB are obtained by minimizing the FB energy with respect to the radius $dE_{\rm FB}/dR = 0$:

$$E_{\rm FB} = \frac{3\pi}{4}\left(\frac{3}{2\pi}\right)^{2/3}\frac{Q_{\rm FB}^{4/3}}{R}\left[1+\frac{4\pi}{9}\left(\frac{2\pi}{3}\right)^{1/3}\frac{R^2T^2}{Q_{\rm FB}^{2/3}}\right] - \frac{3g_\chi^2}{8\pi}\frac{Q_{\rm FB}^2 L_\phi^2}{R^3} + \frac{4\pi}{3}V_0(T)R^3$$

Fermi gas kinetic energy

FB mass profile

- The mass and radius of FB are obtained by minimizing the FB energy with respect to the radius $dE_{\rm FB}/dR = 0$:

$$E_{\rm FB} = \frac{3\pi}{4}\left(\frac{3}{2\pi}\right)^{2/3}\frac{Q_{\rm FB}^{4/3}}{R}\left[1+\frac{4\pi}{9}\left(\frac{2\pi}{3}\right)^{1/3}\frac{R^2T^2}{Q_{\rm FB}^{2/3}}\right] - \frac{3g_\chi^2}{8\pi}\frac{Q_{\rm FB}^2 L_\phi^2}{R^3} + \frac{4\pi}{3}V_0(T)R^3$$

Yukawa potential

FB mass profile

- The mass and radius of FB are obtained by minimizing the FB energy with respect to the radius $dE_{\rm FB}/dR = 0$:

$$E_{\rm FB} = \frac{3\pi}{4}\left(\frac{3}{2\pi}\right)^{2/3}\frac{Q_{\rm FB}^{4/3}}{R}\left[1+\frac{4\pi}{9}\left(\frac{2\pi}{3}\right)^{1/3}\frac{R^2T^2}{Q_{\rm FB}^{2/3}}\right]-\frac{3g_\chi^2}{8\pi}\frac{Q_{\rm FB}^2L_\phi^2}{R^3}+\frac{4\pi}{3}V_0(T)R^3$$

Temperature-dependent potential

FB mass profile

- The mass and radius of FB are obtained by minimizing the FB energy with respect to the radius $dE_{\rm FB}/dR = 0$:

$$E_{\rm FB} = \frac{3\pi}{4}\left(\frac{3}{2\pi}\right)^{2/3}\frac{Q_{\rm FB}^{4/3}}{R}\left[1+\frac{4\pi}{9}\left(\frac{2\pi}{3}\right)^{1/3}\frac{R^2T^2}{Q_{\rm FB}^{2/3}}\right] - \frac{3g_\chi^2}{8\pi}\frac{Q_{\rm FB}^2 L_\phi^2}{R^3} + \frac{4\pi}{3}V_0(T)R^3$$

$$R_{\rm FB} = \left[\frac{3}{16}\left(\frac{3}{2\pi}\right)^{2/3}\frac{Q_{\rm FB}^{4/3}}{V_0}\right]^{1/4}\left[1-\frac{\pi}{6\sqrt{3}}\frac{T^2}{V_0^{1/2}}\right]^{1/2},$$

$$M_{\rm FB} = Q_{\rm FB}\left(12\pi^2 V_0\right)^{1/4}\left(1+\frac{\pi}{4\sqrt{3}}\frac{T^2}{V_0^{1/2}}\right),$$

- FB relic abundance: $\Omega_{\rm FB}h^2 = \frac{M_{\rm FB}\, n_{\rm FB}|_{T_0}}{3M_{\rm Pl}^2(H_0/h)^2}$

FB collapse to PBH

- The mass and radius of FB are obtained by minimizing the FB energy with respect to the radius $dE_{\rm FB}/dR = 0$:

$$E_{\rm FB} = \frac{3\pi}{4}\left(\frac{3}{2\pi}\right)^{2/3}\frac{Q_{\rm FB}^{4/3}}{R}\left[1+\frac{4\pi}{9}\left(\frac{2\pi}{3}\right)^{1/3}\frac{R^2T^2}{Q_{\rm FB}^{2/3}}\right] - \frac{3g_\chi^2}{8\pi}\frac{Q_{\rm FB}^2 L_\phi^2}{R^3} + \frac{4\pi}{3}V_0(T)R^3$$

$$L_\phi(T) \equiv \left(\left.\frac{d^2V_{\rm eff}}{d\phi^2}\right|_{\phi=0}\right)^{-1/2} = \left(2D(T^2 - T_0^2)\right)^{-1/2}$$

- If the FB temperature further cool down, attractive Yukawa potential dominate when $L_\phi \simeq R_{\rm FB}/Q_{\rm FB}^{1/3}$. FB starts collapsing to PBH.

Quartic effective potential

- We consider the finite-temperature quartic effective potential induce the FOPT:

$$V_{\rm eff}(\phi, T) = D(T^2 - T_0^2)\phi^2 - (AT + C)\phi^3 + \frac{\lambda}{4}\phi^4$$

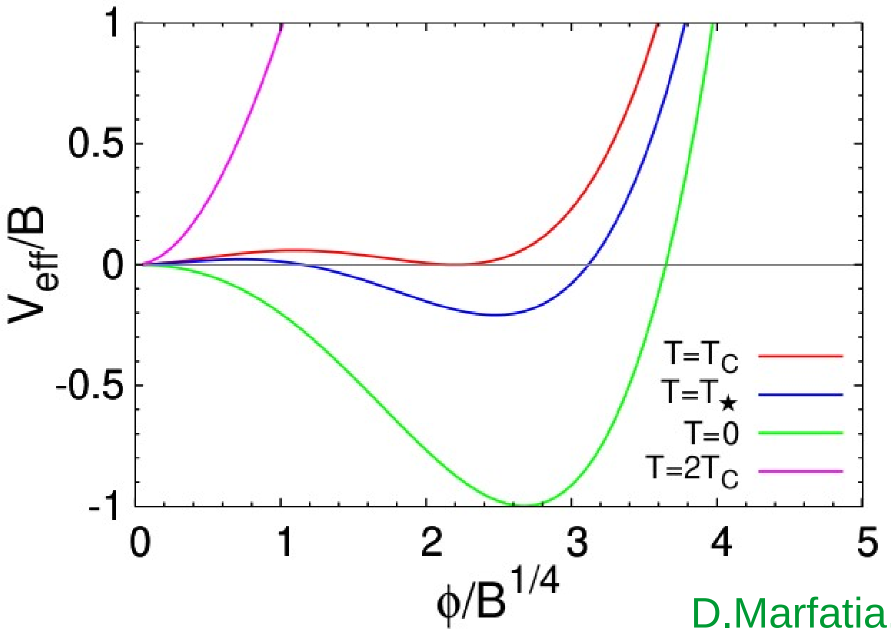

D.Marfatia, P.Y. Tseng: 2107.00859

Signals from FB

Fermi ball

- We consider the finite-temperature quartic effective potential:

D.Marfatia, P.Y. Tseng: 2107.00859

Table 1. Benchmark points with $A = 0.1$. $N_{\rm events}$ is the number of microlensing events expected in 70 hours of observation of M31 by Subaru-HSC.

	BP-1	**BP-2**	**BP-3**	**BP-4**	**BP-5**	**BP-6**	**BP-7**	**BP-8**
λ	0.134	0.158	0.193	0.078	0.062	0.072	0.053	0.060
$B^{1/4}$/keV	2.42	43.5	34.9	64.2	63.6	73.2	284	1390
C/keV	0.059	6.234	4.988	3.080	0.315	0.586	0.342	7.713
D	5.807	0.451	0.720	0.445	0.257	0.293	0.584	0.706
η_χ	7.34×10^{-6}	1.37×10^{-7}	3.51×10^{-6}	4.55×10^{-8}	6.98×10^{-9}	3.64×10^{-9}	8.54×10^{-9}	2.40×10^{-8}
$T_{\rm SM\star}$/keV	1.41	100.0	64.5	128.1	164.8	169.5	427.8	1601
$T_\star$/keV	0.57	34.2	21.6	52.3	84.8	86.9	201.0	879.0
T_f/keV	0.63	41.4	25.9	64.4	92.9	92.5	233.2	1005
$S_3(T_\star)/T_\star$	189	188	187	186	187	184	177	171
$M_{\rm FB}/M_\odot$	3.37×10^{-6}	1.11×10^{-6}	9.66×10^{-6}	1.01×10^{-7}	1.08×10^{-8}	1.08×10^{-9}	9.66×10^{-11}	1.09×10^{-11}
$R_{\rm FB}/R_\odot$	0.529	7.77×10^{-3}	2.15×10^{-2}	2.09×10^{-3}	1.00×10^{-3}	3.86×10^{-4}	2.83×10^{-5}	1.64×10^{-6}
$Q_{\rm FB}$	4.70×10^{56}	8.62×10^{54}	9.38×10^{55}	5.34×10^{53}	5.74×10^{52}	5.00×10^{51}	1.15×10^{50}	2.65×10^{48}
α	1.63×10^{-2}	1.56×10^{-2}	1.70×10^{-2}	2.83×10^{-2}	2.00×10^{-2}	1.24×10^{-2}	1.79×10^{-2}	2.62×10^{-2}
$\beta/H_\star$	3.43×10^4	1.57×10^3	3.01×10^3	2.04×10^3	1.86×10^3	2.80×10^3	4.44×10^3	5.59×10^3
$v_\phi/T_\star$	3.554	4.175	3.958	4.889	3.987	3.501	4.724	4.469
v_w	0.890	0.940	0.937	0.946	0.886	0.854	0.923	0.916
$\Omega_{\rm FB}h^2$	1.79×10^{-2}	5.81×10^{-3}	0.12	2.94×10^{-3}	4.56×10^{-4}	2.70×10^{-4}	2.39×10^{-3}	3.38×10^{-2}
$N_{\rm events}$	19.5	20.4	29.3	38.9	17.5	19.3	46.1	29.1
$\Delta N_{\rm eff}$	0.391	0.226	0.248	0.394	0.497	0.425	0.261	0.408

Fermi ball

- We consider the finite-temperature quartic effective potential:

Input parameters from effective potential

Table 1. Benchmark points with $A = 0.1$. $N_{\rm events}$ is the number of microlensing events expected in 70 hours of observation of M31 by Subaru-HSC.

	BP-1	**BP-2**	**BP-3**	**BP-4**	**BP-5**	**BP-6**	**BP-7**	**BP-8**
λ	0.134	0.158	0.193	0.078	0.062	0.072	0.053	0.060
$B^{1/4}/\text{keV}$	2.42	43.5	34.9	64.2	63.6	73.2	284	1390
C/keV	0.059	6.234	4.988	3.080	0.315	0.586	0.342	7.713
D	5.807	0.451	0.720	0.445	0.257	0.293	0.584	0.706
η_χ	7.34×10^{-6}	1.37×10^{-7}	3.51×10^{-6}	4.55×10^{-8}	6.98×10^{-9}	3.64×10^{-9}	8.54×10^{-9}	2.40×10^{-8}
$T_{\rm SM\star}/\text{keV}$	1.41	100.0	64.5	128.1	164.8	169.5	427.8	1601
$T_\star/\text{keV}$	0.57	34.2	21.6	52.3	84.8	86.9	201.0	879.0
T_f/keV	0.63	41.4	25.9	64.4	92.9	92.5	233.2	1005
$S_3(T_\star)/T_\star$	189	188	187	186	187	184	177	171
$M_{\rm FB}/M_\odot$	3.37×10^{-6}	1.11×10^{-6}	9.66×10^{-6}	1.01×10^{-7}	1.08×10^{-8}	1.08×10^{-9}	9.66×10^{-11}	1.09×10^{-11}
$R_{\rm FB}/R_\odot$	0.529	7.77×10^{-3}	2.15×10^{-2}	2.09×10^{-3}	1.00×10^{-3}	3.86×10^{-4}	2.83×10^{-5}	1.64×10^{-6}
$Q_{\rm FB}$	4.70×10^{56}	8.62×10^{54}	9.38×10^{55}	5.34×10^{53}	5.74×10^{52}	5.00×10^{51}	1.15×10^{50}	2.65×10^{48}
α	1.63×10^{-2}	1.56×10^{-2}	1.70×10^{-2}	2.83×10^{-2}	2.00×10^{-2}	1.24×10^{-2}	1.79×10^{-2}	2.62×10^{-2}
$\beta/H_\star$	3.43×10^{4}	1.57×10^{3}	3.01×10^{3}	2.04×10^{3}	1.86×10^{3}	2.80×10^{3}	4.44×10^{3}	5.59×10^{3}
$v_\phi/T_\star$	3.554	4.175	3.958	4.889	3.987	3.501	4.724	4.469
v_w	0.890	0.940	0.937	0.946	0.886	0.854	0.923	0.916
$\Omega_{\rm FB}h^2$	1.79×10^{-2}	5.81×10^{-3}	0.12	2.94×10^{-3}	4.56×10^{-4}	2.70×10^{-4}	2.39×10^{-3}	3.38×10^{-2}
$N_{\rm events}$	19.5	20.4	29.3	38.9	17.5	19.3	46.1	29.1
$\Delta N_{\rm eff}$	0.391	0.226	0.248	0.394	0.497	0.425	0.261	0.408

Fermi ball

- We consider the finite-temperature quartic effective potential:

Table 1. Benchmark points with $A = 0.1$. N_{events} is the number of microlensing events expected in 70 hours of observation of M31 by Subaru-HSC.

	BP-1	BP-2	BP-3	BP-4	BP-5	BP-6	BP-7	BP-8
λ	0.134	0.158	0.193	0.078	0.062	0.072	0.053	0.060
$B^{1/4}$/keV	2.42	43.5	34.9	64.2	63.6	73.2	284	1390
C/keV	0.059	6.234	4.988	3.080	0.315	0.586	0.342	7.713
D	5.807	0.451	0.720	0.445	0.257	0.293	0.584	0.706
η_χ	7.34×10^{-6}	1.37×10^{-7}	3.51×10^{-6}	4.55×10^{-8}	6.98×10^{-9}	3.64×10^{-9}	8.54×10^{-9}	2.40×10^{-8}
$T_{\text{SM}\star}$/keV	1.41	100.0	64.5	128.1	164.8	169.5	427.8	1601
$T_\star$/keV	0.57	34.2	21.6	52.3	84.8	86.9	201.0	879.0
T_f/keV	0.63	41.4	25.9	64.4	92.9	92.5	233.2	1005
$S_3(T_\star)/T_\star$	189	188	187	186	187	184	177	171
$M_{\text{FB}}/M_\odot$	3.37×10^{-6}	1.11×10^{-6}	9.66×10^{-6}	1.01×10^{-7}	1.08×10^{-8}	1.08×10^{-9}	9.66×10^{-11}	1.09×10^{-11}
$R_{\text{FB}}/R_\odot$	0.529	7.77×10^{-3}	2.15×10^{-2}	2.09×10^{-3}	1.00×10^{-3}	3.86×10^{-4}	2.83×10^{-5}	1.64×10^{-6}
Q_{FB}	4.70×10^{56}	8.62×10^{54}	9.38×10^{55}	5.34×10^{53}	5.74×10^{52}	5.00×10^{51}	1.15×10^{50}	2.65×10^{48}
α	1.63×10^{-2}	1.56×10^{-2}	1.70×10^{-2}	2.83×10^{-2}	2.00×10^{-2}	1.24×10^{-2}	1.79×10^{-2}	2.62×10^{-2}
$\beta/H_\star$	3.43×10^{4}	1.57×10^{3}	3.01×10^{3}	2.04×10^{3}	1.86×10^{3}	2.80×10^{3}	4.44×10^{3}	5.59×10^{3}
$v_\phi/T_\star$	3.554	4.175	3.958	4.889	3.987	3.501	4.724	4.469
v_w	0.890	0.940	0.937	0.946	0.886	0.854	0.923	0.916
$\Omega_{\text{FB}}h^2$	1.79×10^{-2}	5.81×10^{-3}	0.12	2.94×10^{-3}	4.56×10^{-4}	2.70×10^{-4}	2.39×10^{-3}	3.38×10^{-2}
N_{events}	19.5	20.4	29.3	38.9	17.5	19.3	46.1	29.1
ΔN_{eff}	0.391	0.226	0.248	0.394	0.497	0.425	0.261	0.408

FB mass, radius and Q-charge

Fermi ball

- We consider the finite-temperature quartic effective potential:

Table 1. Benchmark points with $A = 0.1$. $N_{\rm events}$ is the number of microlensing events expected in 70 hours of observation of M31 by Subaru-HSC.

	BP-1	BP-2	BP-3	BP-4	BP-5	BP-6	BP-7	BP-8
λ	0.134	0.158	0.193	0.078	0.062	0.072	0.053	0.060
$B^{1/4}$/keV	2.42	43.5	34.9	64.2	63.6	73.2	284	1390
C/keV	0.059	6.234	4.988	3.080	0.315	0.586	0.342	7.713
D	5.807	0.451	0.720	0.445	0.257	0.293	0.584	0.706
η_χ	7.34×10^{-6}	1.37×10^{-7}	3.51×10^{-6}	4.55×10^{-8}	6.98×10^{-9}	3.64×10^{-9}	8.54×10^{-9}	2.40×10^{-8}
$T_{\rm SM\star}$/keV	1.41	100.0	64.5	128.1	164.8	169.5	427.8	1601
$T_\star$/keV	0.57	34.2	21.6	52.3	84.8	86.9	201.0	879.0
T_f/keV	0.63	41.4	25.9	64.4	92.9	92.5	233.2	1005
$S_3(T_\star)/T_\star$	189	188	187	186	187	184	177	171
$M_{\rm FB}/M_\odot$	3.37×10^{-6}	1.11×10^{-6}	9.66×10^{-6}	1.01×10^{-7}	1.08×10^{-8}	1.08×10^{-9}	9.66×10^{-11}	1.09×10^{-11}
$R_{\rm FB}/R_\odot$	0.529	7.77×10^{-3}	2.15×10^{-2}	2.09×10^{-3}	1.00×10^{-3}	3.86×10^{-4}	2.83×10^{-5}	1.64×10^{-6}
$Q_{\rm FB}$	4.70×10^{56}	8.62×10^{54}	9.38×10^{55}	5.34×10^{53}	5.74×10^{52}	5.00×10^{51}	1.15×10^{50}	2.65×10^{48}
α	1.63×10^{-2}	1.56×10^{-2}	1.70×10^{-2}	2.83×10^{-2}	2.00×10^{-2}	1.24×10^{-2}	1.79×10^{-2}	2.62×10^{-2}
$\beta/H_\star$	3.43×10^{4}	1.57×10^{3}	3.01×10^{3}	2.04×10^{3}	1.86×10^{3}	2.80×10^{3}	4.44×10^{3}	5.59×10^{3}
$v_\phi/T_\star$	3.554	4.175	3.958	4.889	3.987	3.501	4.724	4.469
v_w	0.890	0.940	0.937	0.946	0.886	0.854	0.923	0.916
$\Omega_{\rm FB}h^2$	1.79×10^{-2}	5.81×10^{-3}	0.12	2.94×10^{-3}	4.56×10^{-4}	2.70×10^{-4}	2.39×10^{-3}	3.38×10^{-2}
$N_{\rm events}$	19.5	20.4	29.3	38.9	17.5	19.3	46.1	29.1
$\Delta N_{\rm eff}$	0.391	0.226	0.248	0.394	0.497	0.425	0.261	0.408

GW parameters

Gravitational Wave

- GW spectra from the benchmark points:

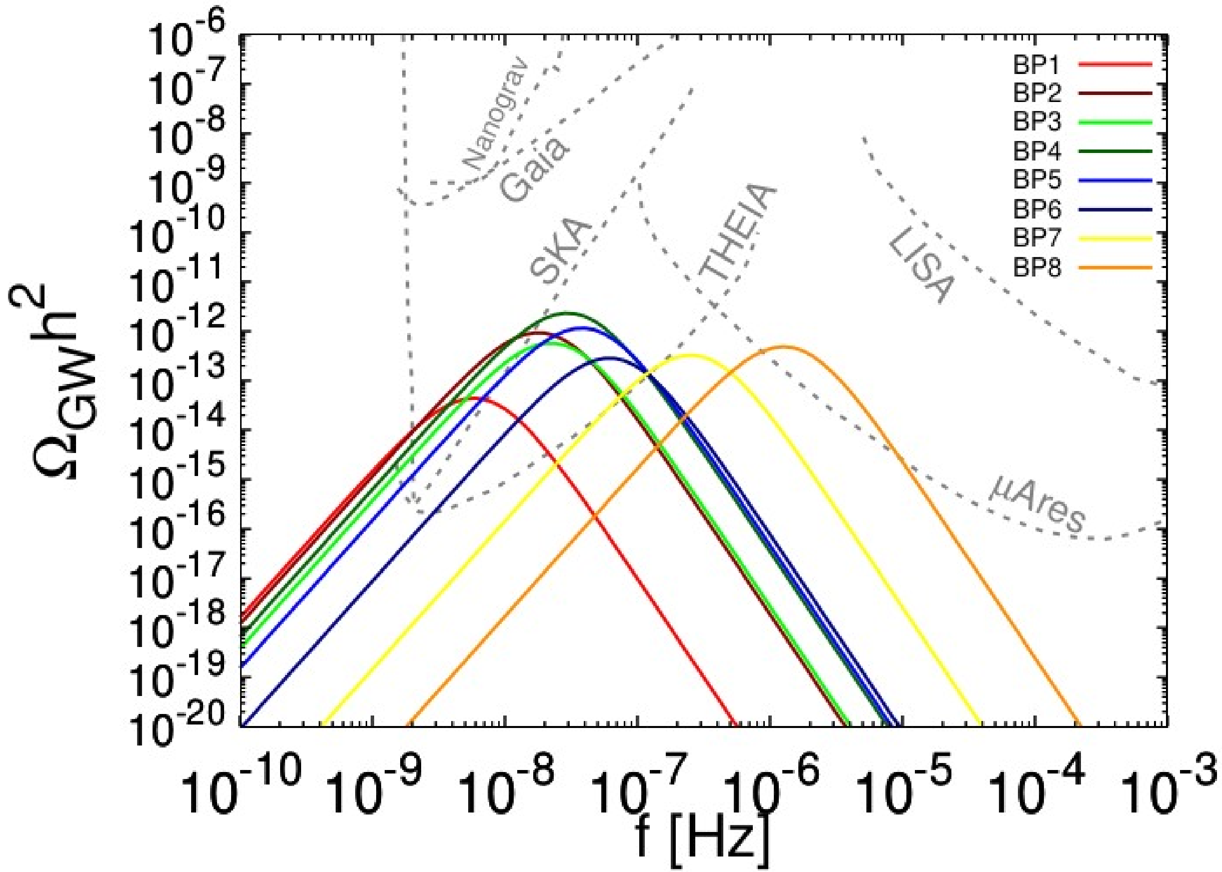

D.Marfatia, P.Y. Tseng: 2107.00859

Gravitational Wave

- GW spectra from the benchmark points:

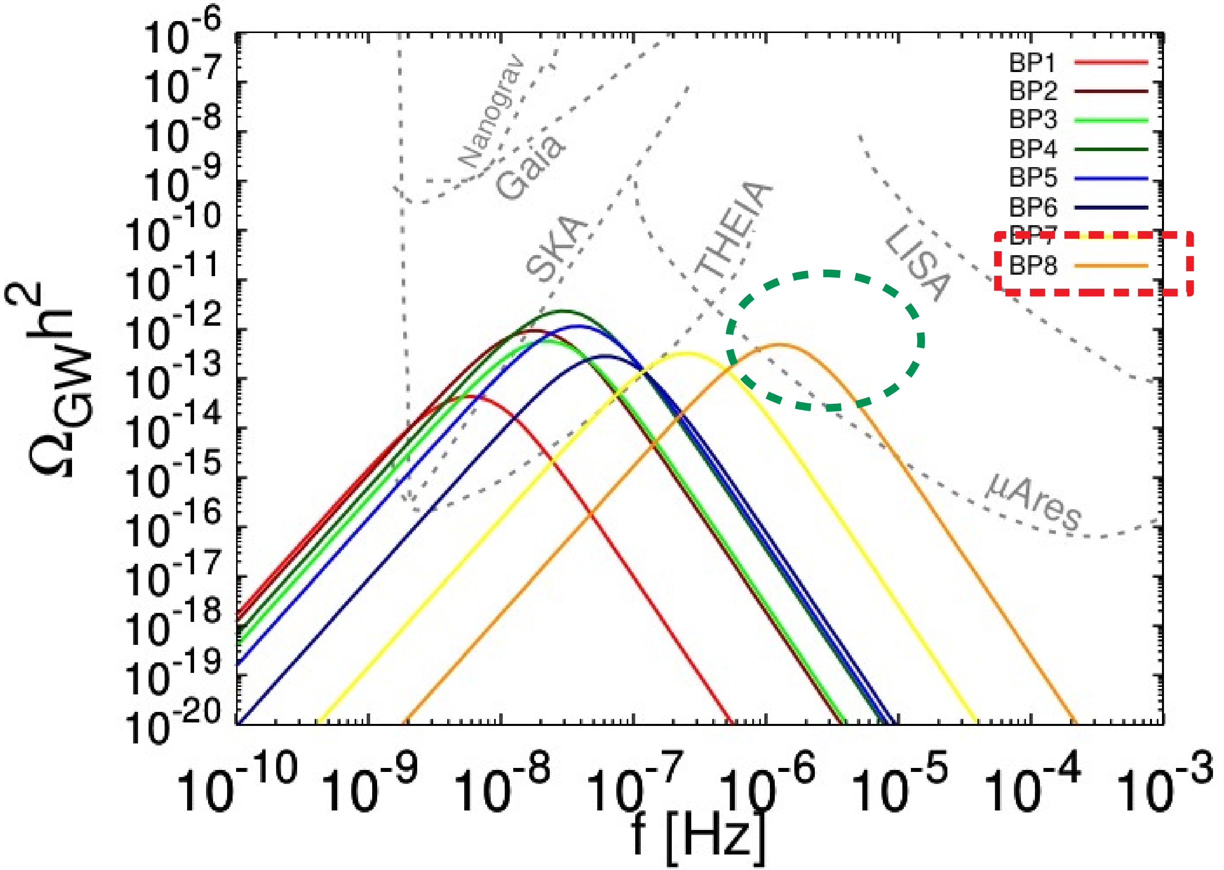

D.Marfatia, P.Y. Tseng: 2107.00859

Microlensing

- These FB mass and radius ranges can induce microlensing effects.

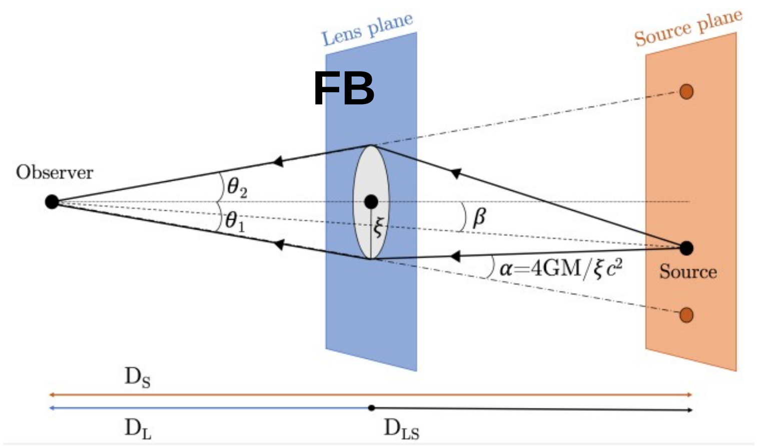

$$\theta_E \equiv \sqrt{\frac{4GM}{c^2}\frac{D_{LS}}{D_L D_S}}$$

$$\mu_{tot} = \frac{u^2+2}{u\sqrt{u^2+4}} \xrightarrow{u=1} 1.34\ .$$

D.Croon, D. McKeen, N. Raj: 2002.08962

- The separating angle of two images of the background star are too small to be resolved, but we can observe the sudden luminosity enhancement of the star.

Microlensing

- Astrophysical Sky surveys are ideal for observing microlensing. Ex. Subaru-HSC (observing M31).

FB halos surround MW and M31. FBs and stars have relative velocity of 250 km/s.

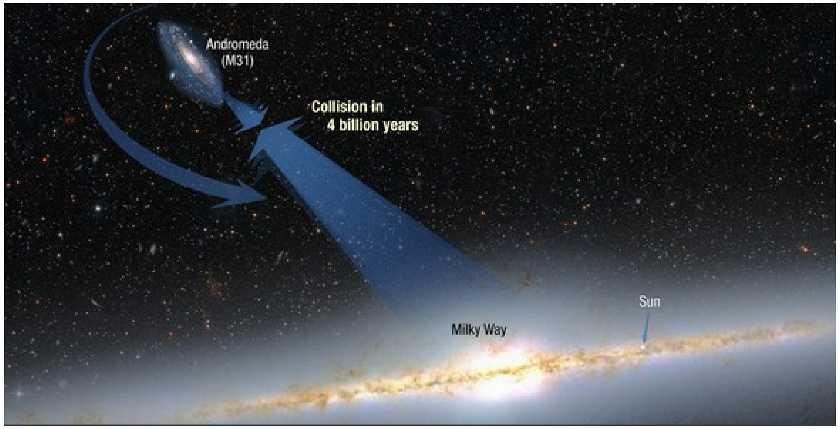

Milky Way Destined for Head-On Collision | NASA

Microlensing

- Astrophysical Sky surveys are ideal for observing microlensing. Ex. Subaru-HSC (observing M31 for 7 hrs).

FB halos surround MW and M31. FBs and stars have relative velocity of 250 km/s.

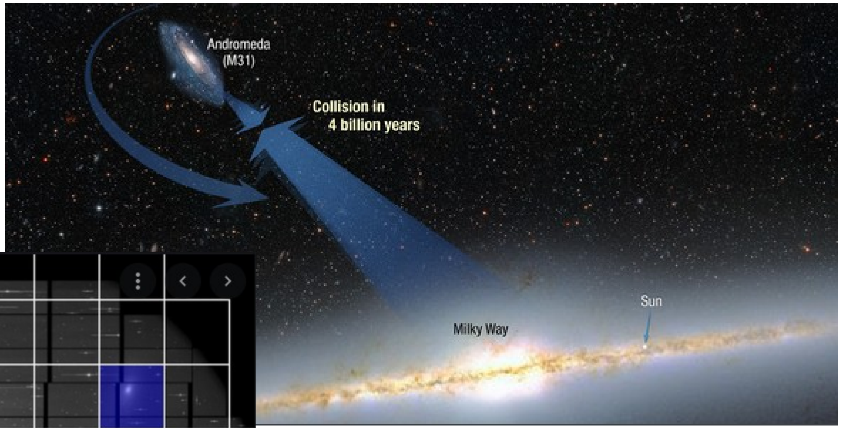

Milky Way Destined for Head-On Collision | NASA

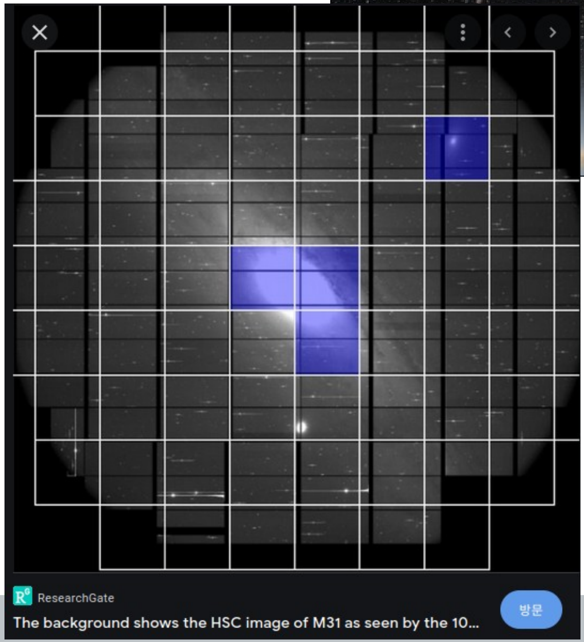

M31 image from Subaru-HSC

Microlensing

- If the lenses have a universal mass $M_{\rm FB}$, with Maxwell-Boltzmann velocity distribution, then event rate per source star is

$$\frac{d^2\Gamma}{dx dt_E} = D_S \frac{f_{\rm DM}}{M_{\rm FB}} \left[\rho^{\rm DM}_{\rm MW}(r_{\rm MW}) \frac{v_E^4}{v_{\rm MW}^2} e^{-v_E^2/v_{\rm MW}^2} + \rho^{\rm DM}_{\rm M31}(r_{\rm M31}) \frac{v_E^4}{v_{\rm M31}^2} e^{-v_E^2/v_{\rm M31}^2} \right]$$

$$v_E(x) = 2u_{1.34}(x) R_E(x)/t_E$$

- The t_E is the time duration for each event.

$$x \equiv D_L/D_S$$

Microlensing

- If the lenses have a universal mass $M_{\rm FB}$, with Maxwell-Boltzmann velocity distribution, then event rate per source star is

$$\frac{d^2\Gamma}{dx dt_E} = D_S \frac{f_{\rm DM}}{M_{\rm FB}} \left[\rho^{\rm DM}_{\rm MW}(r_{\rm MW}) \frac{v_E^4}{v_{\rm MW}^2} e^{-v_E^2/v_{\rm MW}^2} + \rho^{\rm DM}_{\rm M31}(r_{\rm M31}) \frac{v_E^4}{v_{\rm M31}^2} e^{-v_E^2/v_{\rm M31}^2} \right]$$

- Total event rate, we need to sum over the stars in M31

$$N_{\rm events} = N_S T_{\rm obs} \int dt_E \int dR_S \int_0^1 dx \frac{d^2\Gamma}{dx dt_E} \frac{dn}{dR_S}$$

$$N_S = 8.7 \times 10^7$$

$$T_{\rm obs} = 7 \text{ hrs}$$

Microlensing

- The 95% CL on the fractional FB relic abundance $f_{\rm DM}$ requiring $N_{\rm event} \leq 4.74$ corresponds to one observed event at Subaru-HSC:

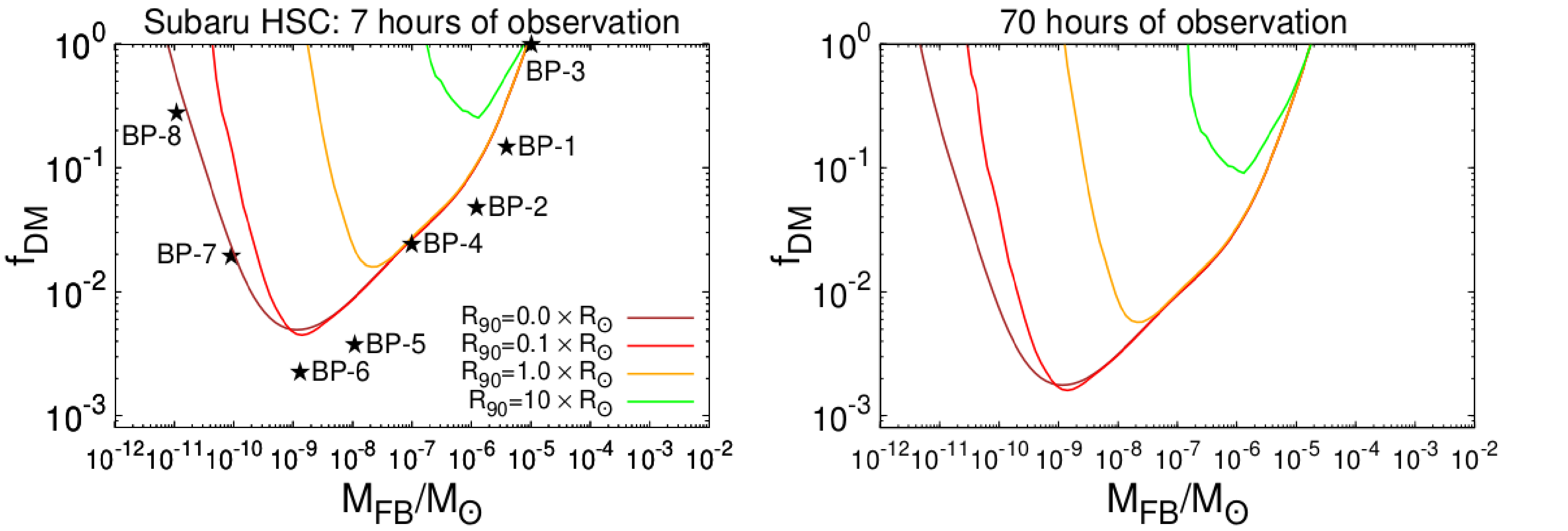

Here we included the finite size effect for microlensing.

Microlensing

- The 95% CL on the fractional FB relic abundance $f_{\rm DM}$ requiring $N_{\rm event} \leq 4.74$ corresponds to one observed event at Subaru-HSC:

$$10^{-12} M_\odot \lesssim M_{\rm FB} \lesssim 10^{-5} M_\odot$$

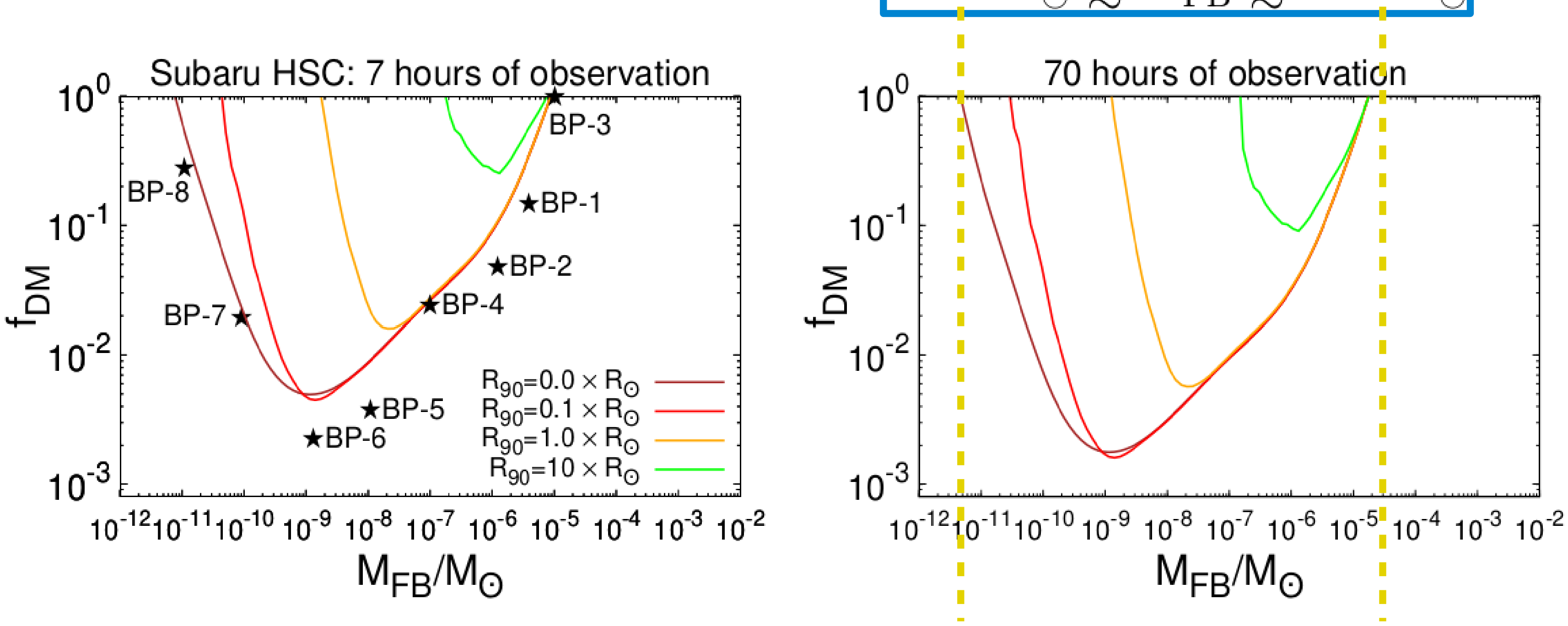

Here we included the finite size effect for microlensing.

Relativistic degree of freedom

- The temperature of FOPT is lower than the BBN, and robust 95% CL upper limit is $\Delta N_{\rm eff} \lesssim 0.5$. 2009.09745, 1103.1261

Table 1. Benchmark points with $A = 0.1$. $N_{\rm events}$ is the number of microlensing events expected in 70 hours of observation of M31 by Subaru-HSC.

	BP-1	BP-2	BP-3	BP-4	BP-5	BP-6	BP-7	BP-8
λ	0.134	0.158	0.193	0.078	0.062	0.072	0.053	0.060
$B^{1/4}$/keV	2.42	43.5	34.9	64.2	63.6	73.2	284	1390
C/keV	0.059	6.234	4.988	3.080	0.315	0.586	0.342	7.713
D	5.807	0.451	0.720	0.445	0.257	0.293	0.584	0.706
η_χ	7.34×10^{-6}	1.37×10^{-7}	3.51×10^{-6}	4.55×10^{-8}	6.98×10^{-9}	3.64×10^{-9}	8.54×10^{-9}	2.40×10^{-8}
$T_{\rm SM\star}$/keV	1.41	100.0	64.5	128.1	164.8	169.5	427.8	1601
$T_\star$/keV	0.57	34.2	21.6	52.3	84.8	86.9	201.0	879.0
T_f/keV	0.63	41.4	25.9	64.4	92.9	92.5	233.2	1005
$S_3(T_\star)/T_\star$	189	188	187	186	187	184	177	171
$M_{\rm FB}/M_\odot$	3.37×10^{-6}	1.11×10^{-6}	9.66×10^{-6}	1.01×10^{-7}	1.08×10^{-8}	1.08×10^{-9}	9.66×10^{-11}	1.09×10^{-11}
$R_{\rm FB}/R_\odot$	0.529	7.77×10^{-3}	2.15×10^{-2}	2.09×10^{-3}	1.00×10^{-3}	3.86×10^{-4}	2.83×10^{-5}	1.64×10^{-6}
$Q_{\rm FB}$	4.70×10^{56}	8.62×10^{54}	9.38×10^{55}	5.34×10^{53}	5.74×10^{52}	5.00×10^{51}	1.15×10^{50}	2.65×10^{48}
α	1.63×10^{-2}	1.56×10^{-2}	1.70×10^{-2}	2.83×10^{-2}	2.00×10^{-2}	1.24×10^{-2}	1.79×10^{-2}	2.62×10^{-2}
$\beta/H_\star$	3.43×10^{4}	1.57×10^{3}	3.01×10^{3}	2.04×10^{3}	1.86×10^{3}	2.80×10^{3}	4.44×10^{3}	5.59×10^{3}
$v_\phi/T_\star$	3.554	4.175	3.958	4.889	3.987	3.501	4.724	4.469
v_w	0.890	0.940	0.937	0.946	0.886	0.854	0.923	0.916
$\Omega_{\rm FB}h^2$	1.79×10^{-2}	5.81×10^{-3}	0.12	2.94×10^{-3}	4.56×10^{-4}	2.70×10^{-4}	2.39×10^{-3}	3.38×10^{-2}
$N_{\rm events}$	19.5	20.4	29.3	38.9	17.5	19.3	46.1	29.1
$\Delta N_{\rm eff}$	0.391	0.226	0.248	0.394	0.497	0.425	0.261	0.408

Temperature of FOPT

Relativistic degree of freedom

- The temperature of FOPT is lower than the BBN, and robust 95% CL upper limit is $\Delta N_{\rm eff} \lesssim 0.5$. 2009.09754:1103.1261

- We consider decoupled dark and SM sectors with temperature ratio $r_T = \frac{T_i^{\rm (D)}}{T^{\rm (SM)}}$.

- The extra effective neutrino number

Y.Nakai,M.Suzuki,F.Takahashi, M.Yamada: 2009.09754

$$\Delta N_{\rm eff} \simeq 0.49 \times \left(\frac{R}{0.13}\right)^{4/3} \left(\frac{g_{*0}^{\rm (D)}}{g_{*0}}\right) \left(\frac{g_{*s0}}{g_{*s0}^{\rm (D)}}\right)^{4/3}$$

$$g_\star^{(D)} = 2*2*(7/8)+1 = 4.5$$

- R is the entropy ratio after the phase transition.

Relativistic degree of freedom

- The temperature of FOPT is lower than the BBN, and robust 95% CL upper limit is $\Delta N_{\rm eff} \lesssim 0.5$.

2009.09754:1103.1261

Table 1. Benchmark points with $A = 0.1$. $N_{\rm events}$ is the number of microlensing events expected in 70 hours of observation of M31 by Subaru-HSC.

	BP-1	**BP-2**	**BP-3**	**BP-4**	**BP-5**	**BP-6**	**BP-7**	**BP-8**
λ	0.134	0.158	0.193	0.078	0.062	0.072	0.053	0.060
$B^{1/4}$/keV	2.42	43.5	34.9	64.2	63.6	73.2	284	1390
C/keV	0.059	6.234	4.988	3.080	0.315	0.586	0.342	7.713
D	5.807	0.451	0.720	0.445	0.257	0.293	0.584	0.706
η_χ	7.34×10^{-6}	1.37×10^{-7}	3.51×10^{-6}	4.55×10^{-8}	6.98×10^{-9}	3.64×10^{-9}	8.54×10^{-9}	2.40×10^{-8}
$T_{\rm SM\star}$/keV	1.41	100.0	64.5	128.1	164.8	169.5	427.8	1601
$T_\star$/keV	0.57	34.2	21.6	52.3	84.8	86.9	201.0	879.0
T_f/keV	0.63	41.4	25.9	64.4	92.9	92.5	233.2	1005
$S_3(T_\star)/T_\star$	189	188	187	186	187	184	177	171
$M_{\rm FB}/M_\odot$	3.37×10^{-6}	1.11×10^{-6}	9.66×10^{-6}	1.01×10^{-7}	1.08×10^{-8}	1.08×10^{-9}	9.66×10^{-11}	1.09×10^{-11}
$R_{\rm FB}/R_\odot$	0.529	7.77×10^{-3}	2.15×10^{-2}	2.09×10^{-3}	1.00×10^{-3}	3.86×10^{-4}	2.83×10^{-5}	1.64×10^{-6}
$Q_{\rm FB}$	4.70×10^{56}	8.62×10^{54}	9.38×10^{55}	5.34×10^{53}	5.74×10^{52}	5.00×10^{51}	1.15×10^{50}	2.65×10^{48}
α	1.63×10^{-2}	1.56×10^{-2}	1.70×10^{-2}	2.83×10^{-2}	2.00×10^{-2}	1.24×10^{-2}	1.79×10^{-2}	2.62×10^{-2}
$\beta/H_\star$	3.43×10^4	1.57×10^3	3.01×10^3	2.04×10^3	1.86×10^3	2.80×10^3	4.44×10^3	5.59×10^3
$v_\phi/T_\star$	3.554	4.175	3.958	4.889	3.987	3.501	4.724	4.469
v_w	0.890	0.940	0.937	0.946	0.886	0.854	0.923	0.916
$\Omega_{\rm FB}h^2$	1.79×10^{-2}	5.81×10^{-3}	0.12	2.94×10^{-3}	4.56×10^{-4}	2.70×10^{-4}	2.39×10^{-3}	3.38×10^{-2}
$N_{\rm events}$	19.5	20.4	29.3	38.9	17.5	19.3	46.1	29.1
$\Delta N_{\rm eff}$	0.391	0.226	0.248	0.394	0.497	0.425	0.261	0.408

Signals from PBH

PBH: benchmark points

- Benchmark points for PBHs from FOPT.

D.Marfatia, P.Y. Tseng:2112.14588

	BP-1	BP-2	BP-3	BP-4	BP-5	BP-6
λ	0.097	0.177	0.084	0.198	0.198	0.077
$B^{1/4}$/MeV	37.89	16.55	3.412	1.843	0.286	2.411
C/MeV	0.551	1.329	0.054	0.260	0.047	0.022
D	1.257	0.138	0.413	0.750	0.794	0.286
g_χ	0.031	0.020	0.187	0.240	0.118	0.164
η_χ	4.97×10^{-9}	4.67×10^{-11}	3.81×10^{-13}	9.40×10^{-16}	1.47×10^{-18}	9.26×10^{-17}
$T_{\mathrm{SM}\star}$/MeV	29.81	53.46	7.821	2.939	0.440	4.979
$T_\star$/MeV	18.72	36.89	3.156	1.126	0.157	2.908
T_f/MeV	19.73	37.13	3.338	1.343	0.214	3.071
T_ϕ/MeV	17.72	21.64	2.737	0.800	0.077	2.361
$S_3(T_\star)/T_\star$	156	161	165	170	180	170
$M_{\mathrm{PBH}}/M_\odot$	3.18×10^{-16}	1.08×10^{-16}	1.07×10^{-17}	1.07×10^{-18}	3.91×10^{-19}	3.99×10^{-20}
Q_{FB}	5.02×10^{42}	1.77×10^{42}	1.14×10^{42}	2.06×10^{41}	4.48×10^{41}	5.00×10^{39}
β'	3.83×10^{-17}	2.02×10^{-19}	8.01×10^{-23}	3.43×10^{-26}	5.45×10^{-30}	1.01×10^{-27}
α	1.26×10^{-2}	1.72×10^{-3}	2.78×10^{-3}	9.23×10^{-3}	1.81×10^{-2}	1.14×10^{-2}
$\beta/H_\star$	1.42×10^{4}	2.55×10^{3}	4.22×10^{3}	2.86×10^{3}	1.90×10^{3}	2.74×10^{3}
v_w	0.840	0.694	0.845	0.935	0.968	0.843
$\Omega_{\mathrm{PBH}}h^2$	0.108	9.74×10^{-4}	1.15×10^{-6}	1.57×10^{-9}	4.17×10^{-13}	2.52×10^{-10}
ΔN_{eff}	0.413	0.406	0.087	0.114	0.165	0.379

PBH: benchmark points

- Benchmark points for PBHs from FOPT.

D.Marfatia, P.Y. Tseng:2112.14588

	BP-1	BP-2	BP-3	BP-4	BP-5	BP-6
λ	0.097	0.177	0.084	0.198	0.198	0.077
$B^{1/4}$/MeV	37.89	16.55	3.412	1.843	0.286	2.411
C/MeV	0.551	1.329	0.054	0.260	0.047	0.022
D	1.257	0.138	0.413	0.750	0.794	0.286
g_χ	0.031	0.020	0.187	0.240	0.118	0.164
η_χ	4.97×10^{-9}	4.67×10^{-11}	3.81×10^{-13}	9.40×10^{-16}	1.47×10^{-18}	9.26×10^{-17}
$T_{\mathrm{SM}\star}$/MeV	29.81	53.46	7.821	2.939	0.440	4.979
$T_\star$/MeV	18.72	36.89	3.156	1.126	0.157	2.908
T_f/MeV	19.73	37.13	3.338	1.343	0.214	3.071
T_ϕ/MeV	17.72	21.64	2.737	0.800	0.077	2.361
$S_3(T_\star)/T_\star$	156	161	165	170	180	170
$M_{\mathrm{PBH}}/M_\odot$	3.18×10^{-16}	1.08×10^{-16}	1.07×10^{-17}	1.07×10^{-18}	3.91×10^{-19}	3.99×10^{-20}
Q_{FB}	5.02×10^{42}	1.77×10^{42}	1.14×10^{42}	2.06×10^{41}	4.48×10^{41}	5.00×10^{39}
β'	3.83×10^{-17}	2.02×10^{-19}	8.01×10^{-23}	3.43×10^{-26}	5.45×10^{-30}	1.01×10^{-27}
α	1.26×10^{-2}	1.72×10^{-3}	2.78×10^{-3}	9.23×10^{-3}	1.81×10^{-2}	1.14×10^{-2}
$\beta/H_\star$	1.42×10^{4}	2.55×10^{3}	4.22×10^{3}	2.86×10^{3}	1.90×10^{3}	2.74×10^{3}
v_w	0.840	0.694	0.845	0.935	0.968	0.843
$\Omega_{\mathrm{PBH}}h^2$	0.108	9.74×10^{-4}	1.15×10^{-6}	1.57×10^{-9}	4.17×10^{-13}	2.52×10^{-10}
ΔN_{eff}	0.413	0.406	0.087	0.114	0.165	0.379

Gravitational Wave

- GW spectra from the benchmark points:

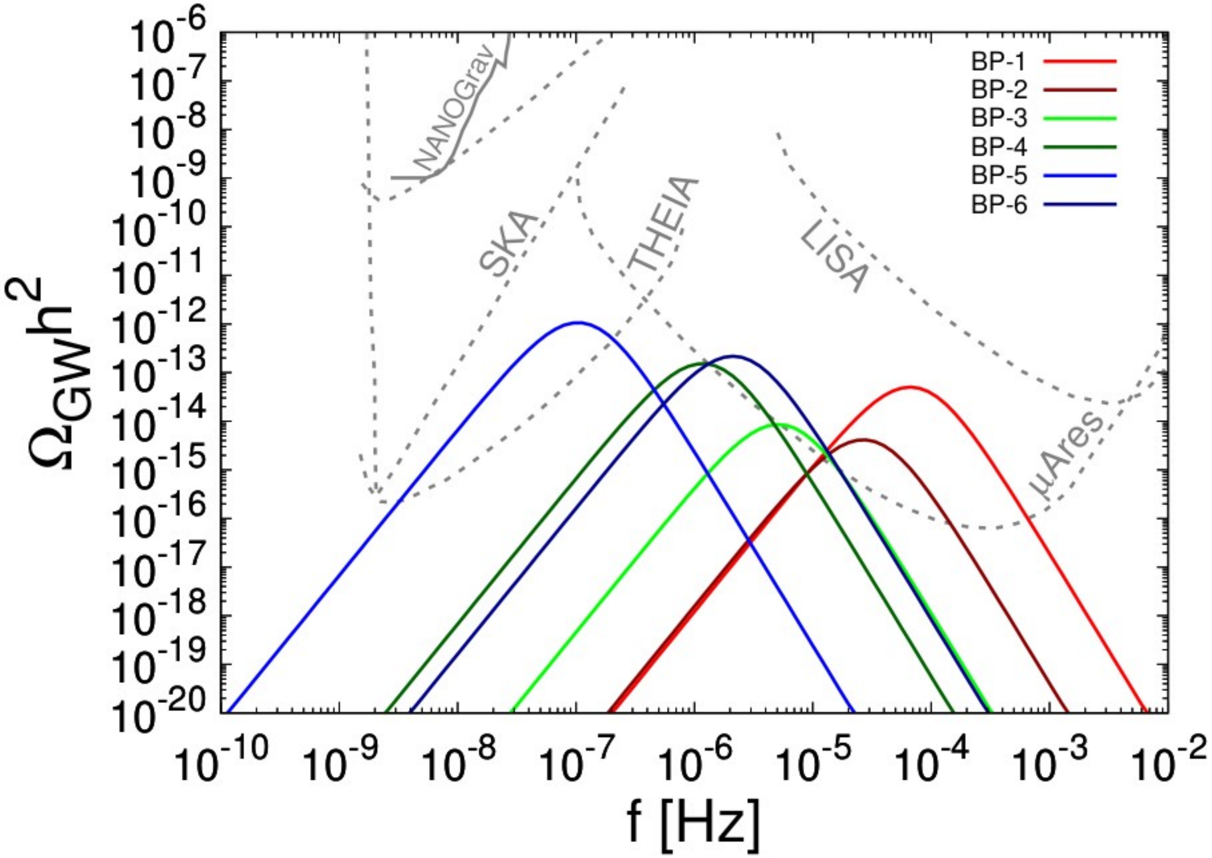

D.Marfatia, P.Y. Tseng: 2112.14588

PBH evaporation

- The evaporation of a PBH produces all particles with mass below the PBH temperature:

$$T_{\rm PBH} \simeq 5.3 \text{ MeV} \times \left(\frac{10^{-18} M_\odot}{M_{\rm PBH}}\right)$$

- For $M_{\rm PBH}/M_\odot \lesssim 10^{-20}$, PBHs evaporated before today.

- The Hawking emission rate of primary particles:

$$\frac{dN_i}{dEdt} = \frac{n_i^{\rm d.o.f}\Gamma_i(E, M_{\rm PBH})}{2\pi(e^{E/T_{\rm PBH}} \pm 1)}$$

PBH evaporation

- The extragalactic gamma-ray background due to PBH evaporation

$$\frac{d^2\Phi}{dEdt} = \int_{t_{\rm CMB}}^{\min(t_{\rm eva},t_0)} c[1+z(t)]\frac{f_{\rm PBH}\rho_{\rm DM}}{M_{\rm PBH}}\frac{d^2N_\gamma}{d\tilde{E}dt}\Big|_{\tilde{E}=[1+z(t)]E} dt$$

with average DM density $\rho_{\rm DM} = 1.27\ {\rm GeV\,m^{-3}}$.

- The evolution of the Universe is approximated as matter dominated until the current epoch

$$1+z(t) = \left(\frac{t_0}{t}\right)^{2/3}$$

PBH evaporation

- The extragalactic gamma-ray background due to PBH evaporation for the benchmark points

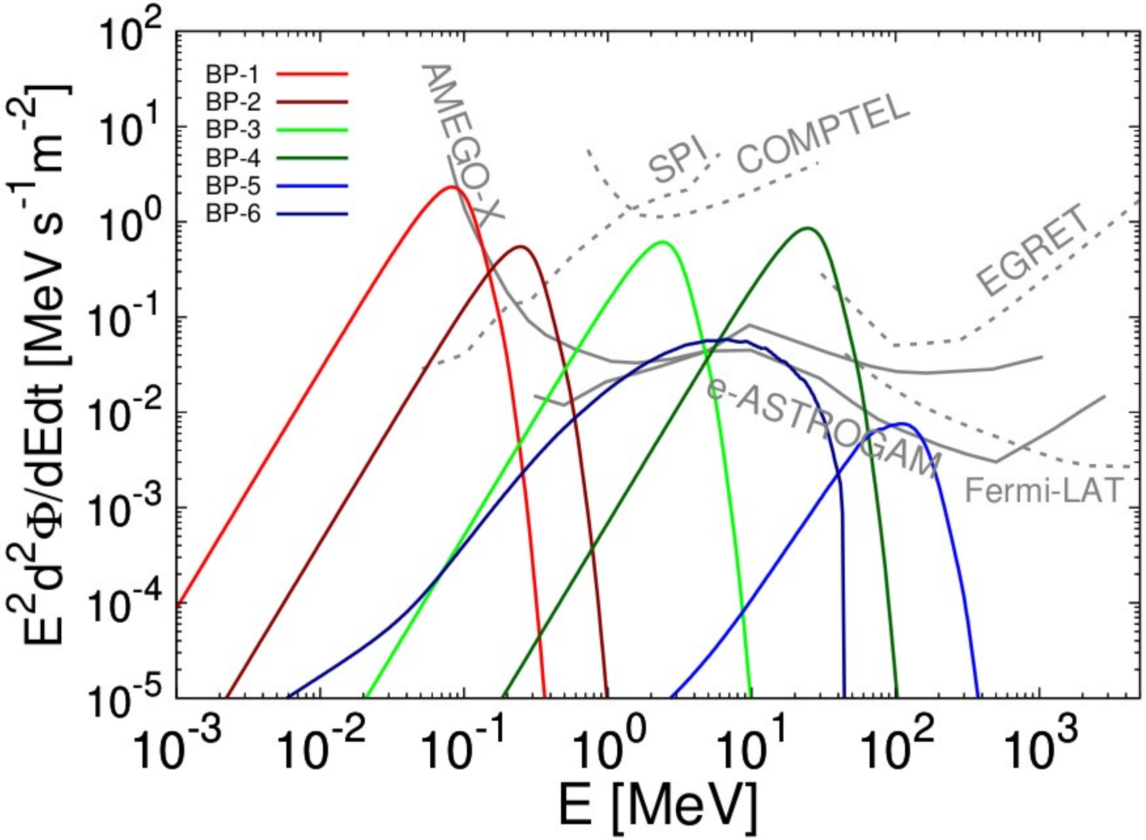

Summary

Summary

- We discuss two scenarios of fermion DM particles undergo FOPT by a quartic effective potential.
- FOPT endows DM mass and induces stochastic background GW signals.
- Fermion DM particles aggregate to form Fermi Ball via FOPT.
- FB of mass $10^{-12} M_\odot \lesssim M_{\rm FB} \lesssim 10^{-5} M_\odot$, correlated observations of GW (10^{-9} Hz – 10^{-5} Hz) from FOPT (*at SKA/THEIA*) and microlensing (*at Subaru-HSC*), can be made.

Summary

- Via the attractive Yukawa potential, FB collapse to PBH.
- In the quartic effective potential framework with vacuum energy difference $0.1 \lesssim B^{1/4}/\mathrm{MeV} \lesssim 10^4$, it produces PBHs of mass $10^{-20} M_\odot \lesssim M_{\mathrm{PBH}} \lesssim 10^{-15} M_\odot$.
- The correlated observations of GW (10^{-7} Hz – 10^{-4} Hz) from FOPT (*at THEIA*, *muAres*) and extragalactic MeV gamma-ray (*at AMEGO-X*, *e-ASTROGAM*), can be made.

Thank you for your attention!

Back up

Part-1: Bubble wall velocity

- Particles reflected by the bubble wall exert pressure on it, and slow down the bubble wall velocity.

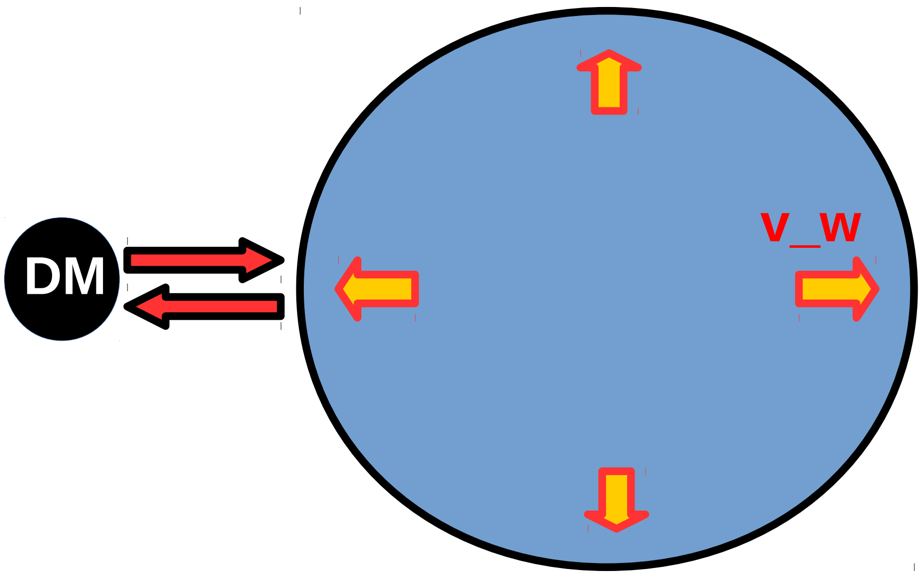

Part-1: Bubble filtering

- If a thermal DM flux is incident on the wall, the number density of DM that enter the bubble is:

$$n_\chi^{\rm in} = n_{\bar\chi}^{\rm in} \simeq \frac{g_{\rm DM} T_\star^3}{\gamma_w v_w} \left(\frac{\gamma_w (1 - v_w) m_\chi / T_\star + 1}{4\pi^2 \gamma_\omega^3 (1 - v_w)^2} \right) e^{-\frac{\gamma_w (1 - v_w) m_\chi}{T_\star}}$$

D.Chway, T.H.Jung, C.S.Shin: 1912.04238

- DMs are filtered by the non-relativistic and relativistic bubble wall velocity:

$$n_\chi^{\rm in} = \begin{cases} \sim e^{-m_\chi / T_\star} & \text{for} \quad v_w \to 0 \\ \sim e^{-m_\chi / (2\gamma_w T_\star)} & \text{for} \quad m_\chi / (\gamma_w T_\star) \to 0 \end{cases}$$

Part-1: Bubble filtering

- If $T_\star < T_{\rm dec}$, the DM inside the bubble is decoupled from the thermal bath and become DM relic abundance.

- DM relic abundance today can be calculated by dividing $n_\chi^{\rm in}+n_{\bar\chi}^{\rm in}$ by entropy $s = (2\pi^2/45)g_{\star S}T^3$:

$$\Omega_{\rm DM}h^2 \simeq 6.29\times 10^8\,\frac{m_\chi(n_\chi^{\rm in}+n_{\bar\chi}^{\rm in})}{\rm GeV}\,\frac{1}{g_{\star S}T_\star^3}$$

$$\Omega_{\rm DM}h^2 \simeq \begin{cases} 1.27\times 10^8\left(\frac{m_\chi}{\rm GeV}\right)\left(\frac{g_{\rm DM}}{g_{\star S}}\right)\left(\frac{m_\chi}{2\gamma_w T_\star}+1\right)e^{-\frac{m_\chi}{2\gamma_w T_\star}}\,, & \text{for } v_w \to 1 \\ 3.19\times 10^7\left(\frac{m_\chi}{\rm GeV}\right)\left(\frac{g_{\rm DM}}{g_{\star S}}\right)\left(\frac{1}{v_w}\right)\left(\frac{m_\chi}{T_\star}+1\right)e^{-\frac{m_\chi}{T_\star}}\,, & \text{for } v_w \to 0. \end{cases}$$

Part-1: Bubble filtering

- If $T_\star < T_{\rm dec}$, the DM inside the bubble is decoupled from the thermal bath and become DM relic abundance.
- DM relic abundance today can be calculated by dividing $n_\chi^{\rm in}+n_{\bar\chi}^{\rm in}$ by entropy $s = (2\pi^2/45) g_{\star S} T^3$:
- For example: $m_\chi \simeq 1~{\rm TeV},\ v_w \to 1$ requires

$$\boxed{\frac{m_\chi}{2\gamma_w T_\star} \simeq 27}$$

Part-1: Bubble filtering

- If $T_\star < T_{\rm dec}$, the DM inside the bubble is decoupled from the thermal bath and become DM relic abundance.
- DM relic abundance today can be calculated by dividing $n_\chi^{\rm in}+n_{\bar\chi}^{\rm in}$ by entropy $s = (2\pi^2/45) g_{\star S} T^3$:

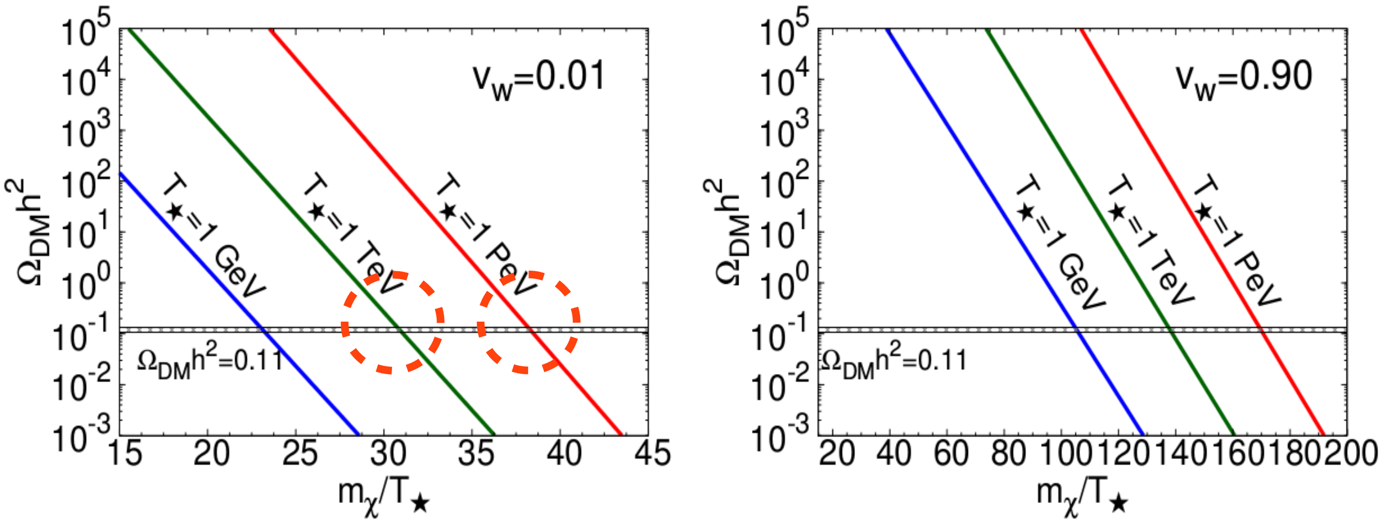

Part-1: Bubble filtering

- Sudden DM freeze-out induced by a FOPT can easily accommodate DM mass above a PeV, which is beyond the current DM direct detection and LHC searches.

- We focus on the Gravitational Wave (GW) signals of Sudden DM freeze-out with a FOPT.

Part-1: Gravitational wave production

- A FOPT generates GWs from three processes: I). Bubble collisions, II). Sound wave in the plasma, III) Magnetohydrodynamic (MHD) turbulence.

- The relevant parameters are required to calculate the GW signals:

$$
\begin{cases}
T_\star\,, \\
\alpha \equiv \dfrac{\left(1 - T\frac{\partial}{\partial T}\right)\Delta V_{\text{eff}}|_{T_\star}}{\rho(T_\star)}\,, \quad \rho \equiv \pi^2 g_\star T^4/30 \\
\dfrac{\beta}{H_\star} \simeq T_\star \dfrac{d(S_3/T)}{dT}\bigg|_{T_\star} \\
v_w
\end{cases}
$$

Part-1: Gravitational wave production

- A FOPT generates GWs from three processes: I). Bubble collisions, II). Sound wave in the plasma, III) Magnetohydrodynamic (MHD) turbulence.

- The Euclidean action:

$$S_3(T) = 4\pi \int_0^\infty r^2 dr \left[\frac{1}{2} \left(\frac{d\phi}{dr} \right)^2 + V_{\rm eff}(\phi, T) \right]$$

- Bubble nucleation rate per unit volume:

$$\Gamma(T) = T^4 \left(\frac{S_3}{2\pi T} \right)^{3/2} e^{-\frac{S_3}{T}}$$

Part-1: Gravitational wave production

- A FOPT generates GWs from three processes: I). Bubble collisions, II). Sound wave in the plasma, III) Magnetohydrodynamic (MHD) turbulence.

- The fraction of space in the false vacuum:

$$F(t) = \exp\left[-\frac{4\pi}{3} v_w^3 \int_{t_c}^{t} dt' (t - t')^3 \Gamma(t')\right]$$

- The percolation temperature $T_\star$ of FOPT is determined by :

$$F(t_\star) = 1/e \simeq 0.37$$

Part-1: Gravitational wave production

- A FOPT generates GWs from: I). Bubble collisions

$$h^2\Omega_{\rm env}(f) = 1.67\times10^{-5}\left(\frac{H_*}{\beta}\right)^2\left(\frac{\kappa\alpha}{1+\alpha}\right)^2\left(\frac{100}{g_*}\right)^{\frac{1}{3}}\left(\frac{0.11\,v_w^3}{0.42+v_w^2}\right)S_{\rm env}(f)$$

C.Caprini et. al: 1512.06239

$$S_{\rm env}(f) = \frac{3.8\,(f/f_{\rm env})^{2.8}}{1+2.8\,(f/f_{\rm env})^{3.8}}$$

- The peak frequency is determined by the time scale of FOPT $1/\beta$:

$$\frac{f_*}{\beta} = \left(\frac{0.62}{1.8-0.1v_w+v_w^2}\right)$$

Part-1: Gravitational wave production

- A FOPT generates GWs from: I). Bubble collisions

$$h^2\Omega_{\rm env}(f) = 1.67\times 10^{-5}\left(\frac{H_*}{\beta}\right)^2\left(\frac{\kappa\alpha}{1+\alpha}\right)^2\left(\frac{100}{g_*}\right)^{\frac{1}{3}}\left(\frac{0.11\,v_w^3}{0.42+v_w^2}\right) S_{\rm env}(f)$$

C.Caprini et. al: 1512.06239

$$S_{\rm env}(f) = \frac{3.8\,(f/f_{\rm env})^{2.8}}{1+2.8\,(f/f_{\rm env})^{3.8}}$$

- The peak frequency is determined by the time scale of FOPT. Then red-shift to present epoch

$$f_{\rm env} = 16.5\times 10^{-3}\,{\rm mHz}\left(\frac{f_*}{\beta}\right)\left(\frac{\beta}{H_*}\right)\left(\frac{T_*}{100\,{\rm GeV}}\right)\left(\frac{g_*}{100}\right)^{\frac{1}{6}}$$

Part-1: Scalar quartic Model

- The finite-temperature quartic effective scalar potential is:

$$V_{\rm eff}(\eta, T) = \frac{\mu^2 + DT^2}{2}\eta^2 - \xi T\eta^3 + \frac{\lambda}{4}\eta^4$$

F.C.Adams: hep-ph/9302321

- Including one-loop Coleman-Weinberg and finite-temperature contributions, potentials of this form are commonly found in *inert singlet*, *inert doublet*, *MSSM*, *and Majoron models*.

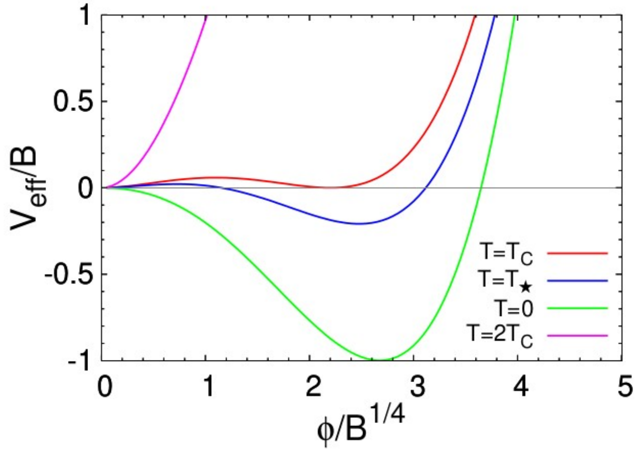

Part-1: Scalar quartic Model

- The finite-temperature quartic effective scalar potential is:

$$V_{\rm eff}(\eta, T) = \frac{\mu^2 + DT^2}{2}\eta^2 - \xi T \eta^3 + \frac{\lambda}{4}\eta^4$$

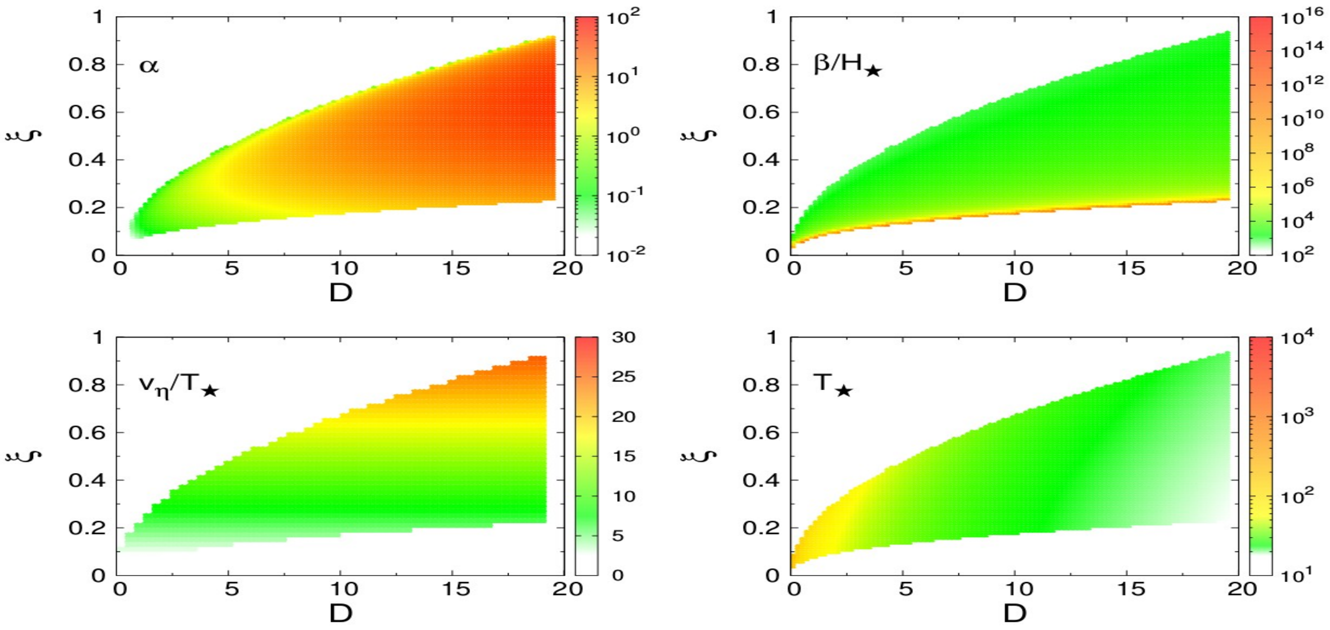

Figure 2. The parameters α, β/H, $v_\eta/T_\star$, and $T_\star$ for the Scalar Quartic Model with $\lambda = 0.1$.

D.Marfatia, P.Y. Tseng: 2006.07313

Part-1: Scalar quartic Model

- The finite-temperature quartic effective scalar potential is:

$$V_{\text{eff}}(\eta, T) = \frac{\mu^2 + DT^2}{2}\eta^2 - \xi T\eta^3 + \frac{\lambda}{4}\eta^4$$

- Correct DM relic:

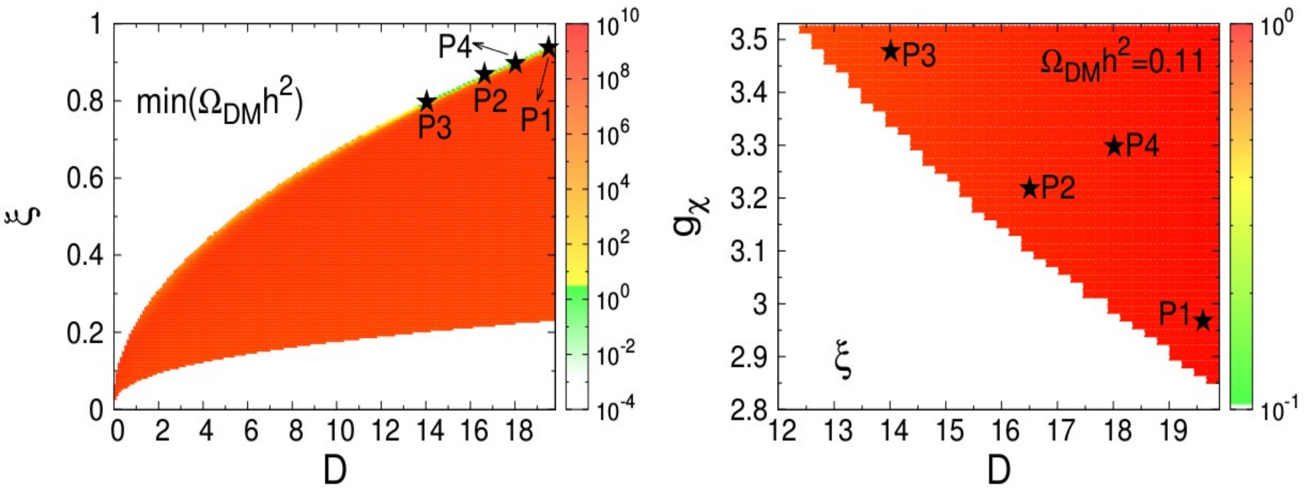

D.Marfatia, P.Y. Tseng: 2006.07313

Part-1: Scalar quartic Model

- The finite-temperature quartic effective scalar potential is:

$$V_{\text{eff}}(\eta, T) = \frac{\mu^2 + DT^2}{2}\eta^2 - \xi T\eta^3 + \frac{\lambda}{4}\eta^4$$

- Benchmark points:

Table 1. Benchmark points (with $\lambda = 0.1$) for the Scalar Quartic Model that give $\Omega_{\text{DM}}h^2 = 0.11$.

	P1	**P2**	**P3**	**P4**
ξ	0.943	0.863	0.796	0.901
D	19.7	16.5	14.0	18.0
g_χ	2.97	3.22	3.48	3.31
α	0.089	0.082	0.076	0.121
$\beta/H_\star$	1116	1062	1015	1085
$v_\eta/T_\star$	25.71	23.41	21.49	24.51
v_w	0.768	0.763	0.760	0.791
$T_\star$/GeV	21.5	23.8	26.1	22.7
m_χ/GeV	1642	1799	1953	1838

D.Marfatia, P.Y. Tseng: 2006.07313

Part-1: Scalar quartic Model

- The finite-temperature quartic effective scalar potential is:

$$V_{\rm eff}(\eta, T) = \frac{\mu^2 + DT^2}{2}\eta^2 - \xi T\eta^3 + \frac{\lambda}{4}\eta^4$$

- GW signals:

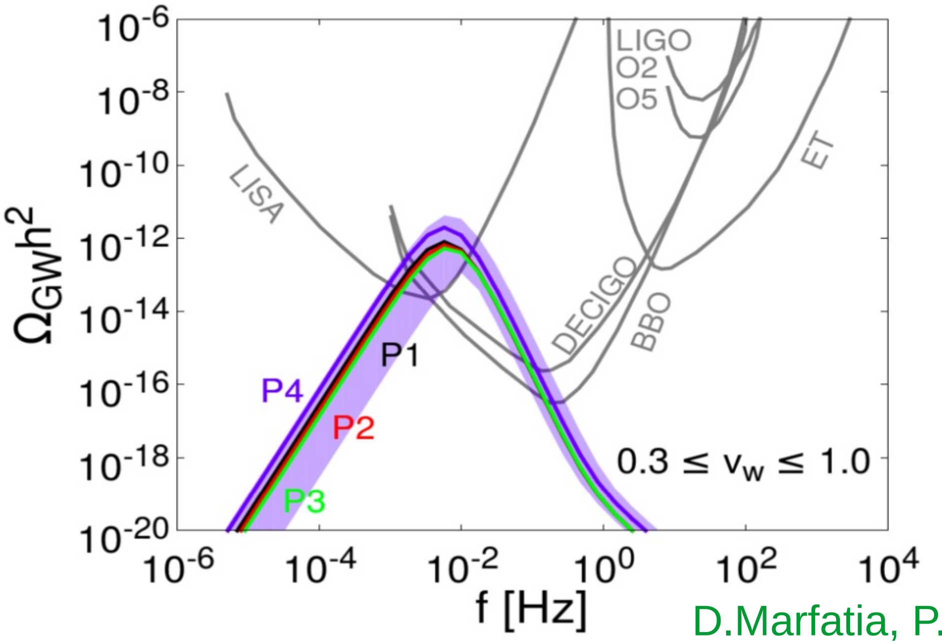

D.Marfatia, P.Y. Tseng: 2006.07313

Part-1: Summary

- We studied the sudden freeze-out DM as an alternative to the continuous thermal freeze-out.
- A necessary ingredient is a FOPT generates DM mass.
- The DM relic abundance may be determined by bubble filtering.
- Because FOPT triggers sudden DM freeze-out, GW offers a signature.

Part-1: Introduction

- The $m_\chi/T_\star$ needed to produce the DM relic abundance depends on the velocity of bubble wall v_w .

$$T_\star = m_\chi/30 \text{ for } m_\chi = 1 \text{ TeV}, v_w = 0.01$$

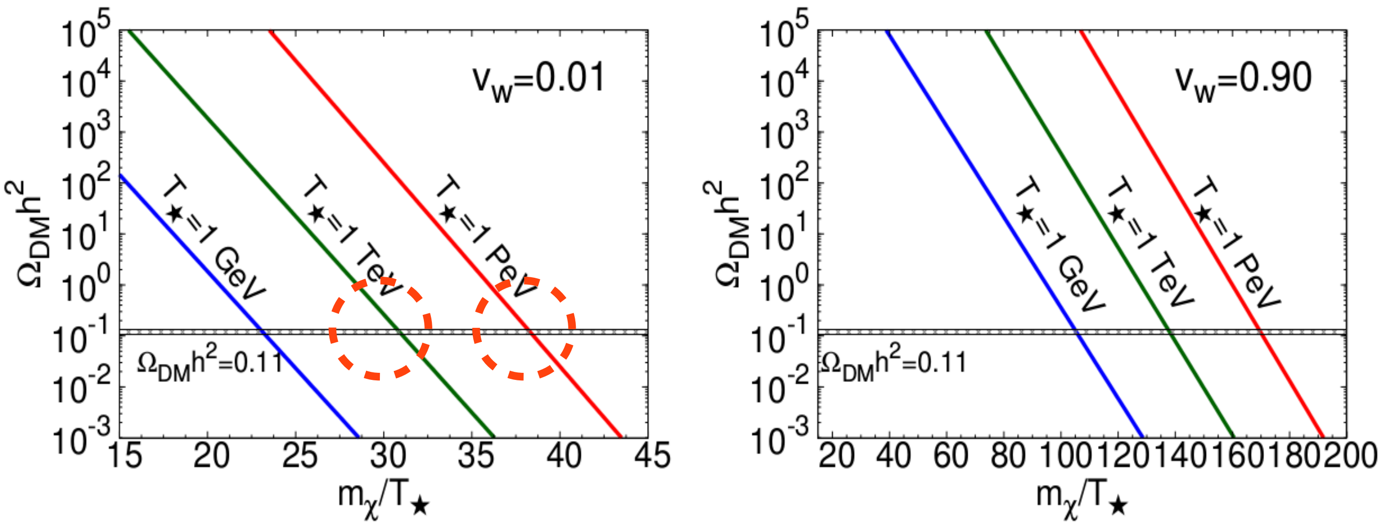

Part-1: Bubble wall velocity

- In the ultrarelativistic limit, the pressure on bubble wall can be obtain from the light degree of freedom inside and outside the bubble:

D.Chway et.al : 1912.04238
J.R.Espinosa et.al: 1004.4187
D.Bodeker et.al : 0903.4099

$$P = \frac{d_n g_\star \pi^2}{90}(1+v_w)^3\gamma_\omega^2 T_\star^4$$

$$d_n \equiv \frac{1}{g_\star}\left[\sum_{0.2M_i>\gamma_w T_\star}\left(g_i^b + \frac{7}{8}g_i^f\right)\right]$$

- The v_w can be obtained by solving the eq. $P = \Delta V_{\rm eff}$:

$$\alpha = \frac{d_n}{3}(1+v_w)^3\gamma_\omega^2$$

$$\alpha \equiv \frac{\left(1-T\frac{\partial}{\partial T}\right)\Delta V_{\rm eff}|_{T_\star}}{\rho(T_\star)}, \quad \rho \equiv \pi^2 g_\star T^4/30$$

Part-1: Bubble wall velocity

- For bubble wall velocity v_w faster than the sound speed in plasma, but not ultrarelativistic, we use the approximation:

P.J.Steinhardt, Phys. Rev. D. 25, 2074 (1982)

$$v_w = \frac{\frac{1}{\sqrt{3}} + \sqrt{\alpha^2 + \frac{2}{3}\alpha}}{1+\alpha}$$

Part-2: anti-correlation

- The percolation condition using saddle point approximation:

$$F(t) = \exp\left[-\frac{4\pi}{3} v_w^3 \int_{t_c}^{t} dt'(t-t')^3 \Gamma(t')\right] \qquad F(t_\star) = 1/e \simeq 0.37$$

$$8\pi v_w^3 \Gamma(T_\star)\beta^{-4} \simeq 1$$

- Since $\beta/H_\star$ is almost constant, thus $\beta \propto H_\star \propto T_\star^2$ and from above condition, we have

$$T_\star^{-4}\, e^{-S_3(T_\star)/T_\star} \simeq B^{-1}\, e^{-S_3(T_\star)/T_\star} \simeq \text{constant}\,, \quad \text{i.e.,} \quad e^{-S_3(T_\star)/T_\star} \propto B$$

- Bubble nucleation rate per unit volume grow with vacuum energy density.

- For fixed $\Omega_{\rm FB} h^2$, we obtain $M_{\rm FB} \propto 1/n_{\rm FB}|_{T_0} \propto e^{3/4 \cdot (S_3(T_\star)/T_\star)} \propto B^{-3/4}$

Part-2: Anti-correlation

- We consider the finite-temperature quartic effective potential.
- Anti-correlation between the FB mass and energy scale of FOPT.

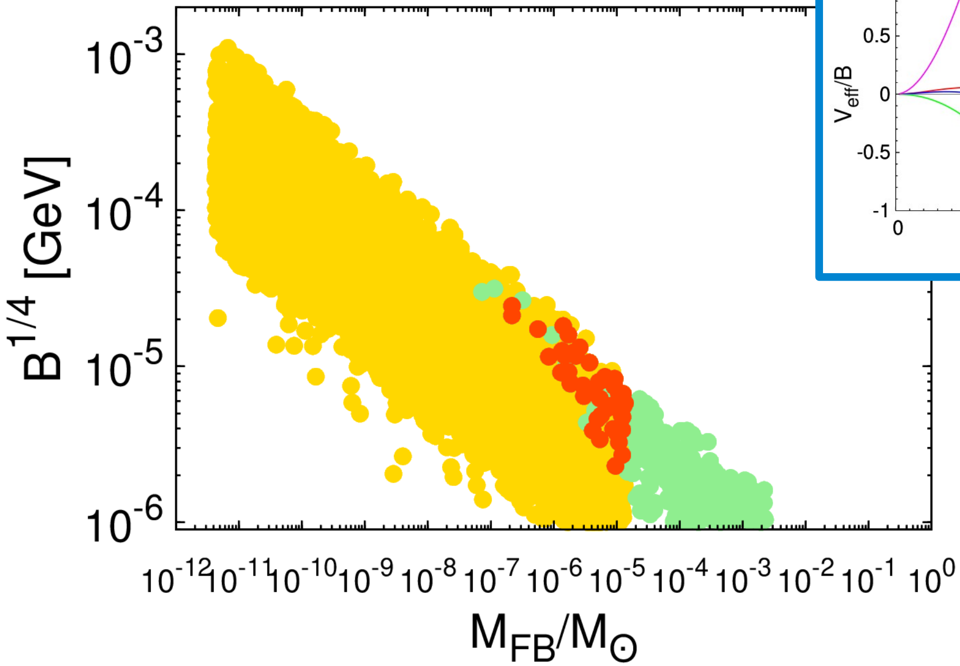

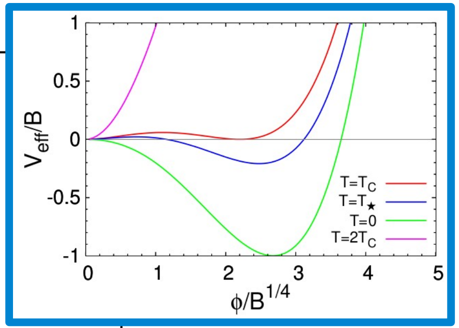

Part-2: Number density of FB

- Solving the Tolman-Oppenheimer-Volkoff(TOV) equation to find the density profile of FB

D.Marfatia, P.Y. Tseng: 2107.00859

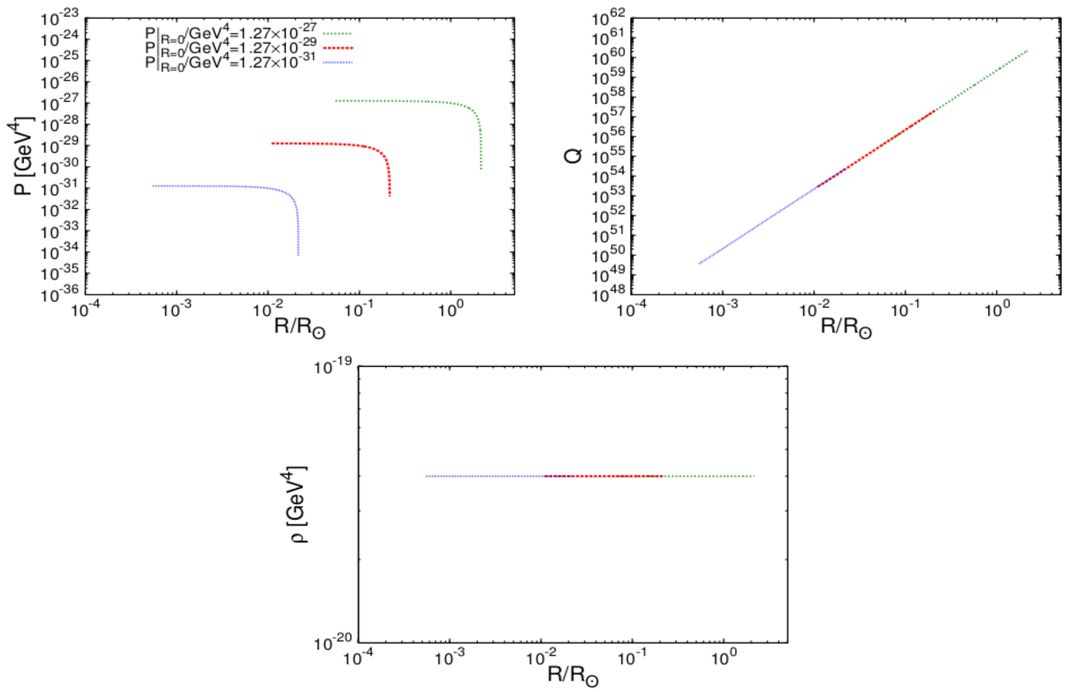

Figure 2. The pressure P (upper-left), Q-charge within radius R (upper-right), and energy density profile (bottom) of a FB with $B^{1/4} = 10$ keV for three boundary conditions, $P|_{R=0} = 1.27 \times 10^{-27}$ GeV^4, $P|_{R=0} = 1.27 \times 10^{-29}$ GeV^4, and $P|_{R=0} = 1.27 \times 10^{-31}$ GeV^4. Correspondingly, $(M_{\rm FB}/M_\odot, R_{\rm FB}/R_\odot) = (6.5079 \times 10^{-2}, 2.149)$, $(6.4911 \times 10^{-5}, 0.2149)$, and $(6.5079 \times 10^{-8}, 2.149 \times 10^{-2})$.

Part-2: Correlated signals

- From BBN, the robust 95% CL upper limit is $\Delta N_{\rm eff} \lesssim 0.5$.

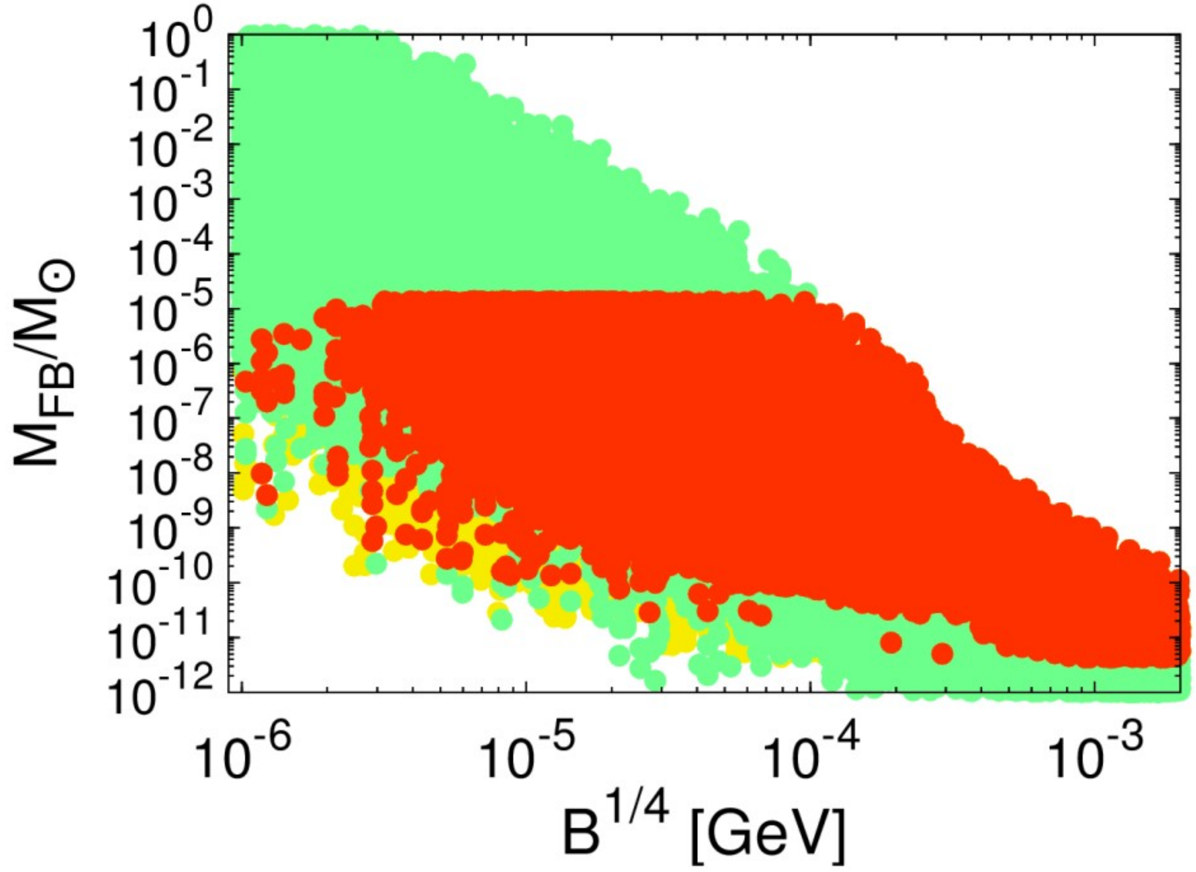

Yellow: microlensing
Green: GW
Red: GW+microlensing

Part-2: Microlensing

- If the lenses have a universal mass $M_{\rm FB}$, with Maxwell-Boltzmann velocity distribution, then event rate per source star is

$$\frac{d^2\Gamma}{dx dt_E} = D_S \frac{f_{\rm DM}}{M_{\rm FB}} \left[\rho^{\rm DM}_{\rm MW}(r_{\rm MW}) \frac{v_E^4}{v^2_{\rm MW}} e^{-v_E^2/v^2_{\rm MW}} + \rho^{\rm DM}_{\rm M31}(r_{\rm M31}) \frac{v_E^4}{v^2_{\rm M31}} e^{-v_E^2/v^2_{\rm M31}} \right]$$

$$v_E(x) = 2u_{1.34}(x) R_E(x)/t_E$$

- The t_E is the time duration for each event.

$$x \equiv D_L/D_S$$

u1.34=1 for point-like lens and background star.

Part-2: Microlensing

- If the lenses have a universal mass $M_{\rm FB}$, with Maxwell-Boltzmann velocity distribution, then event rate per source star is

$$\frac{d^2\Gamma}{dx dt_E} = D_S \frac{f_{\rm DM}}{M_{\rm FB}} \left[\rho^{\rm DM}_{\rm MW}(r_{\rm MW}) \frac{v_E^4}{v_{\rm MW}^2} e^{-v_E^2/v_{\rm MW}^2} + \rho^{\rm DM}_{\rm M31}(r_{\rm M31}) \frac{v_E^4}{v_{\rm M31}^2} e^{-v_E^2/v_{\rm M31}^2} \right]$$

$$v_E(x) = 2u_{1.34}(x) R_E(x)/t_E$$

- The radius distribution of stars in M31:

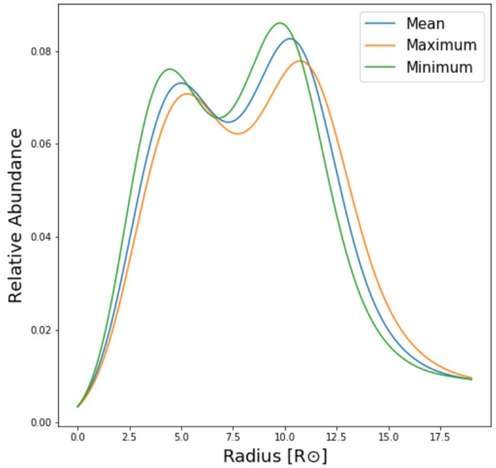

N.Smyth et.al: 1910.01285

Part-2: Microlensing: Finit-size

- Finite-size effect:

D.Croon, D.McKeen, N.Raj, and Z.Wang: 2007.12697

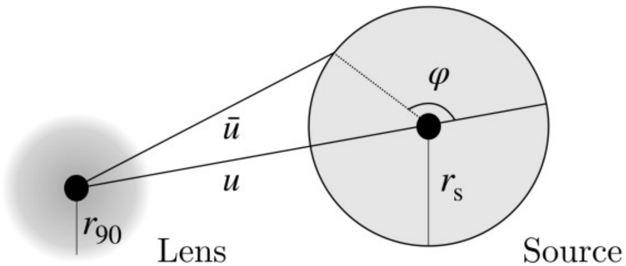

$$\bar{u}(\varphi) = \sqrt{u^2 + r_S^2 + 2ur_S\cos\varphi}$$

- Solve the lens equation for along the edge of the source:

$$\bar{u}(\varphi) = t(\varphi) - \frac{m(t(\varphi))}{t(\varphi)}$$

- The magnification is the area of each image:

$$\mu_i = \eta\frac{1}{\pi r_S^2}\int_0^\pi t_{\varphi,i}^2(\psi)d\psi$$

$$\psi = \tan^{-1}\frac{r_S\sin\varphi}{u + r_S\cos\varphi}, \quad 0 \leq \psi \leq \pi$$

Part-2: Microlensing: Finit-size

- Finite-size effect:

D.Croon, D.McKeen, N.Raj, and Z.Wang: 2007.12697

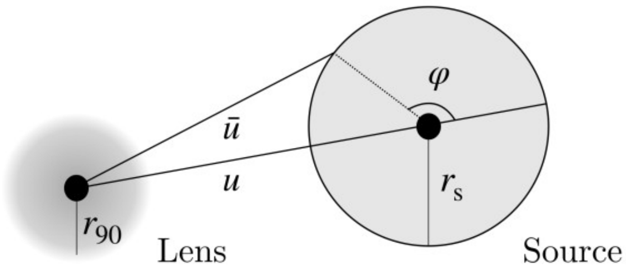

$$\bar{u}(\varphi) = \sqrt{u^2 + r_S^2 + 2ur_S\cos\varphi}$$

- The effective size for 1.34 times magnification:

$$\mu_{tot}(u \leq u_{1.34}) \geq 1.34$$

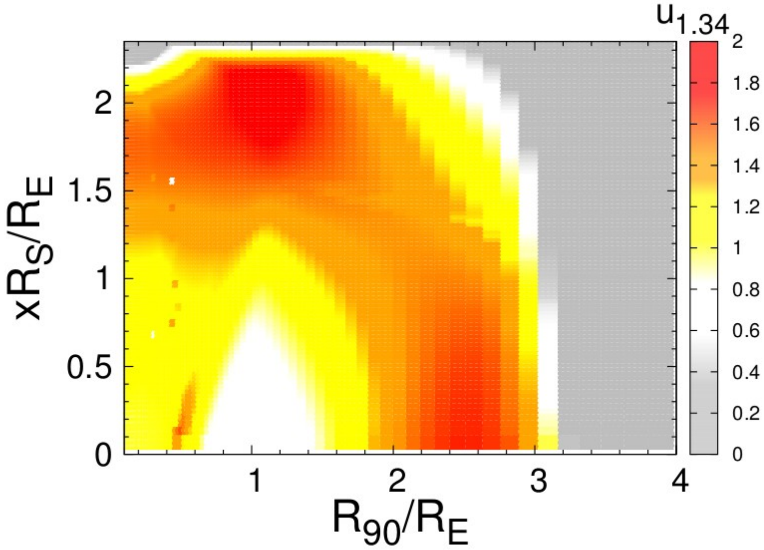

D.Marfatia, P.Y. Tseng: 2107.00859

Part-2: Microlensing

- If the lenses have a universal mass $M_{\rm FB}$, with Maxwell-Boltzmann velocity distribution, then event rate per source star is

$$\frac{d^2\Gamma}{dx dt_E} = D_S \frac{f_{\rm DM}}{M_{\rm FB}} \left[\rho^{\rm DM}_{\rm MW}(r_{\rm MW}) \frac{v_E^4}{v_{\rm MW}^2} e^{-v_E^2/v_{\rm MW}^2} + \rho^{\rm DM}_{\rm M31}(r_{\rm M31}) \frac{v_E^4}{v_{\rm M31}^2} e^{-v_E^2/v_{\rm M31}^2} \right]$$

$$v_E(x) = 2u_{1.34}(x) R_E(x)/t_E$$

- Finite-size effect:

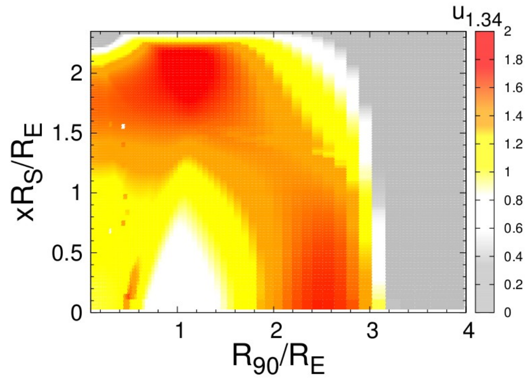

D.Marfatia, P.Y. Tseng: 2107.00859

Part-2: Correlated signals

- Correlated signals of GW and microlensing:

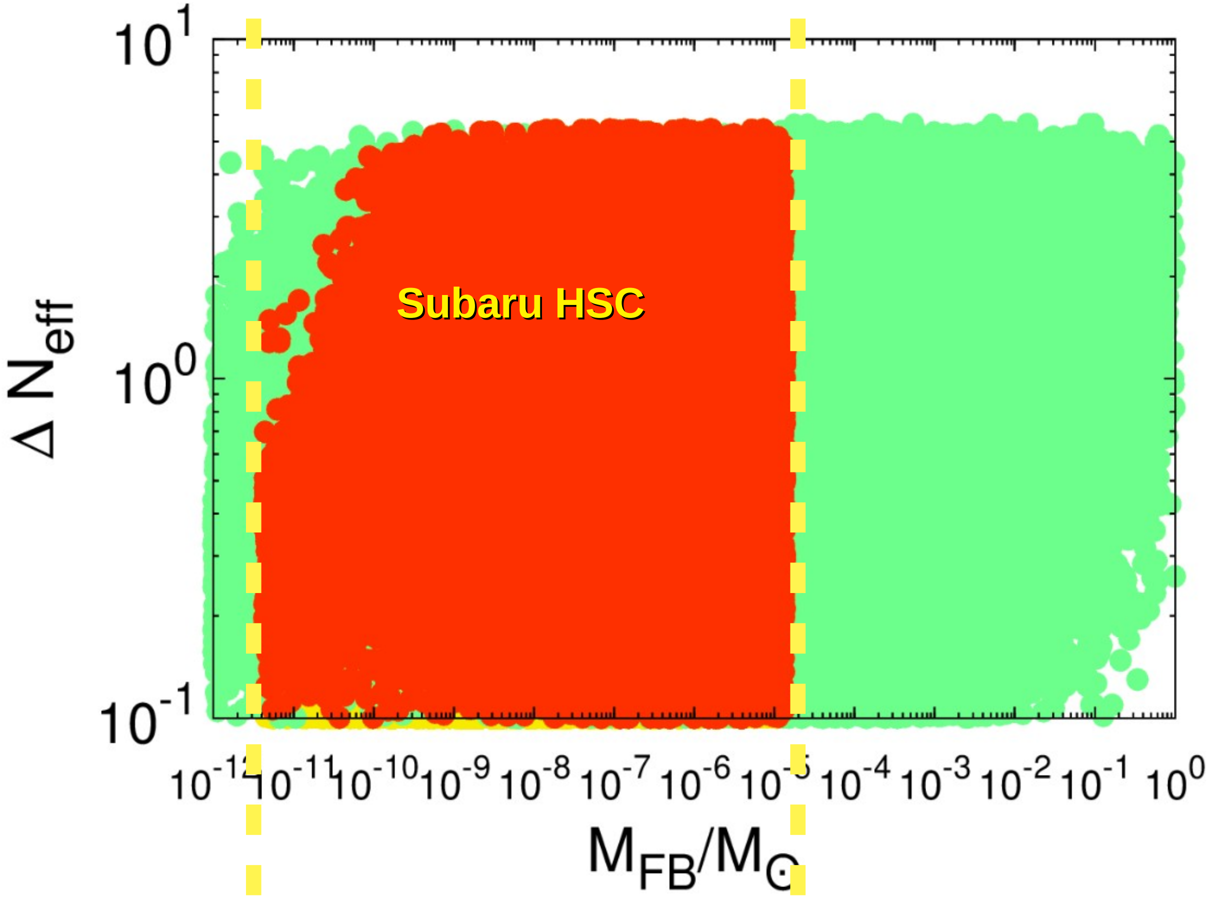

Yellow: microlensing
Green: GW
Red: GW+microlensing

Part-2: Correlated signals

- Correlated signals of GW and microlensing:

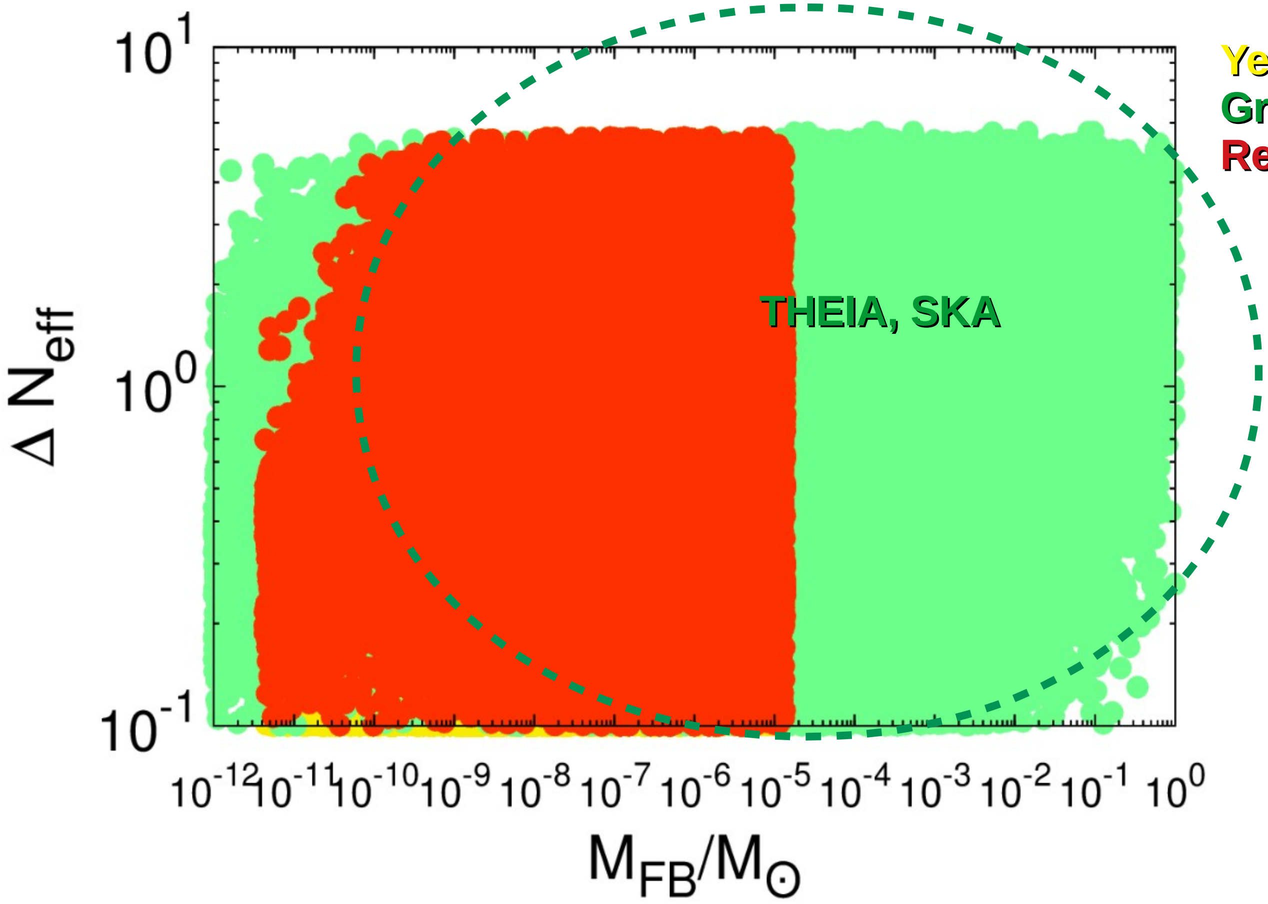

Yellow: microlensing
Green: GW
Red: GW+microlensing

Part-2: Correlated signals

- Correlated signals of GW and microlensing:

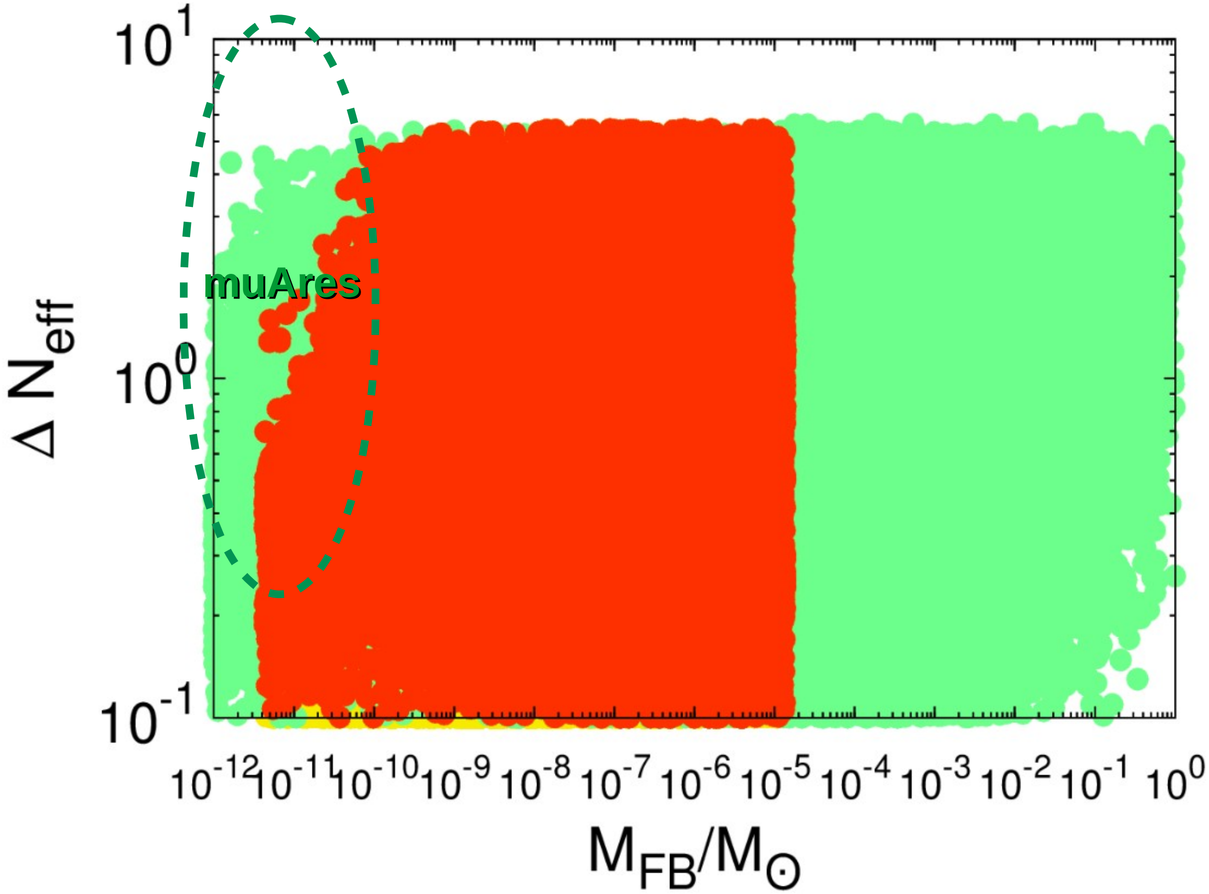

Yellow: microlensing
Green: GW
Red: GW+microlensing

Part-2: Correlated signals

- From BBN, the robust 95% CL upper limit is $\Delta N_{\rm eff} \lesssim 0.5$.